# IRIS

Master thesis in Petroleum Engineering

Computation of the relationship between interfacial area, capillary pressure and saturation in porous media based on the level set method

*Stavanger*

*June 2012*

Zana (Pepaj) Pepic

*University of Stavanger*

Supervisor:       Dr. Johan Olav Helland

Department of Petroleum recovery, COREC

International Research Institute of Stavanger


Faculty supervisor:   Professor Svein Skjæveland

Department of Petroleum Engineering

University of Stavanger

# ACKNOWLEDGMENT

I would like to first and foremost thank my supervisor at the International Research Institute of Stavanger, Dr. Johan Olav Helland, for constructive and fruitful discussions during the work of this study. I would not be able to finish had it not been for the ongoing motivation and help from him.

I would also like to thank my faculty supervisor at the University of Stavanger, Professor Svein Skjæveland, for giving me the opportunity to write this thesis.

Great appreciation goes to the International Research Institute of Stavanger for allowing me to spend endless hours simulating on their computers.

I also thank my father, Bedria Pepaj, for whom I owe a great appreciation for and also my mother, Selvija, for encouraging me and feeding me well during the work of this thesis. I also thank the rest of my family for inspiring me to finish. And last but not least my friends for their friendship and support, sometimes at very late hours on campus.

# ABSTRACT

To gain a better understanding of the relationship between capillary pressure, water saturation and interfacial area in two phase flow, we have studied the drainage and imbibition process for an oil-water system. A level set model that was developed at IRIS was used to simulate the results, which where plotted in Excel and Matlab. Furthermore Paraview was used to visualize the oil migration for the imbibition and drainage process.

The capillary pressure curves showed to differ when the invasion of the fluid occurred from different sides in the heterogeneous rock. Furthermore the result obtained showed that inclusion of the interfacial area in the capillary pressure and water saturation relationship did not eliminate hysteresis.

# Table of Contents

# LIST OF FIGURES

# NOMENCLATURE

| | |
|---|---|
| $A_{f-f}$ | interfacial area between any fluid-fluid interaction |
| $A_{ow}$ | interfacial area between oil and water |
| $a_{ow}$ | specific interfacial area between oil and water |
| C | interface curvature |
| $P_c$ | capillary pressure |
| $P_o$ | oil pressure |
| $P_w$ | water pressure |
| $P_{nw}$ | capillary pressure in nonwetting fluid |
| $P_w$ | capillary pressure in wetting fluid |
| $\sigma_{f_{nw},f_w}$ | interfacial tension between the nonwetting and wetting fluid |
| $r_{nw}$ | principal radii of the curvature for the nonwetting fluid |
| $r_w$ | principal radii of the curvature for the wetting fluid |
| $r_m$ | mean radius of curvature |
| $S_w$ | water saturation |
| $S_o$ | oil saturation |
| $V_v$ | volume of the void space |
| $V_o$ | volume of oil in the pore space |
| $\sigma_{os}$ | interfacial energy between oil and solid |
| $\sigma_{ow}$ | interfacial energy between oil and water |
| $\sigma_{sw}$ | interfacial energy between solid and water |
| $\theta$ | contact angle |
| $d(\vec{x})$ | distance function |
| $\varphi$ | signed distance function |
| $\varphi_{ow}$ | the signed distance function for oil/water interface |
| $\varphi_{vs}$ | the signed distance function for void/solid interface |
| $S(\varphi)$ | sign function |
| $\varepsilon$ | tolerance value |
| H | the Heaviside function |
| $\delta$ | the Dirac delta function |

| | |
|---|---|
| $\partial\Omega$ | interface boundary |
| $\Omega^+$ | exterior |
| $\Omega^-$ | interior |
| $\vec{N}$ | normal vector |
| $\vec{T}$ | tangential vector |
| $V_n$ | interface speed in normal direction |
| $V_t$ | interface speed in tangential direction |
| $\kappa$ | mean interface curvature |
| HJ WENO | Hamilton Jacobi Weighted Essentially Nonoscillatory |
| TVD RK | Total Variation Diminishing Runga-Kutta |
| CFL | Courant-Friedreich-Levy |
| $b$ | b-factor |
| $N$ | number of grid points |
| IFA | interfacial area |

Subscripts

| | |
|---|---|
| $f$ | fluid |
| $o$ | oil |
| $w$ | water |
| $s$ | solid |
| $v$ | void |
| $c$ | capillary |
| $n$ | normal direction |
| $t$ | tangential direction |

# CHAPTER 1

# INTRODUCTION

Fluid interactions are important in the petroleum industry and other fields such as image processing, computer graphics, computational physics and the list goes on (Helland et al. 2011). In many industries the interactions between immiscible fluids on a microscopic level is important to understand for a series of natural and technical processes. However to investigate fluid interactions at microscopic level is not always an easy task. In the petroleum industry the main focus is usually the interactions between the two immiscible fluids oil and water. The thermodynamic process associated with these two immiscible fluids in the porous media is the capillary induced forces (Morrow et al. 1970). Example is the movement of oil within the porous solids naturally due to pressure differences or forced during water injection. Furthermore a number of experiments have been conducted to explain the relationship between the capillary pressure and water saturation during fluid movement. The characteristic shapes of the drainage and imbibition curves for fluid displacement are well known figures. The shape however depends on the restriction of displacement of the immiscible fluid in the porous media and it may give rise to capillary hysteresis. Capillary hysteresis is due to many factors that govern in the porous media, such as pore connectivity and pore geometry. However the lack of information about the microscale geometry and the microscale processes limit our understanding of the multiphase flow (Culligan et al. 2006). Variables such as the porosity and saturation are defined at macroscopic level. However they might not have a meaning on microscale level (Culligan et al. 2006). The article by *Hassanizadeh and Gray* [1993] proposed an inclusion of the interfacial area between two immiscible fluids to the capillary pressure and water saturation relationship. So that it would aid to eliminate or diminish capillary hysteresis, and relate a macroscopic variable such as the water saturation to a microscopic one. Furthermore the latter work by Joekar-Niasar et al. [2007] showed that the interfacial area could be an essential variable to the $P_c - S_w$ relationship for eliminating hysteresis.

The main objective of this work is to study the relationship between the capillary pressure, water saturation and interfacial area with help of the level set model developed at IRIS. The model developed at IRIS uses the level set method to find results for the capillary pressure, water saturation and interfacial area between oil and water. The model is tested to

whether it simulates results according to experimental results, and if the result obtained can be used to determine if in fact adding the micrcoscopic variable to the $P_c - S_w$-relationship will eliminate hysteresis.

To be able to investigate whether the model produces theoretically correct results compared to experimental data, the drainage and imbibition curves for invasion in different sides of a cube where simulated. The data results where visualized in Paraview to recognize a number of well-known capillary hysteresis events. Furthermore analytical calculations of the interfacial area between oil and water were also conducted to compare with simulations.

# CHAPTER 2

# LITERATURE REVIEW

The basic concepts that are related to this study are elaborated in the following chapter.

## 2.1 Capillary pressure

In oil migration the capillary pressure is an important factor that needs to be studied in detail. The reservoir consists of many fractures with dimensions of tens of microns or less, and the capillary pressure play a significant role in determining the fluid configurations (Prodanovic et al. 2007). The capillary pressure can either aid or oppose the displacement of one fluid by another in the pores of a porous media. The pressure arises when two immiscible fluids come in contact combined with the pore size, pore geometry and the wetting characteristics of the fluids (Wendebourg et al. 1997). Amongst the wetting characteristics the surface and interfacial tensions of the rock and fluids play an important part for the generation of the capillary pressure. The curved surface between the two immiscible fluids will contract into the smallest possible area per unit volume depending on the wettability of the fluid (Tarek et al. 2010). Figure 2.1 is shown to be able to fully understand the concept.
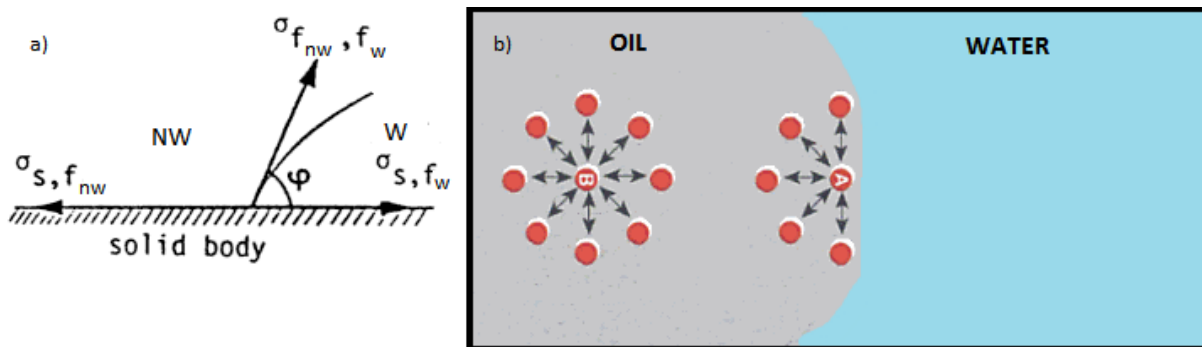


**Figure 2.1:** *a) Interfacial equilibrium between the contact point of two fluids at the surface of a solid body (Bear et al. 1991) b) Intermolecular interaction A) in the interface between oil and water, B) in the oil phase (Schwartzstein et al. 2005).*

As shown in the figure 2.1a the interface between the two immiscible fluids, $f_{nw}, f_w$, is curved where $nw$ and $w$ denotes nonwetting and wetting, respectively. Figure 2.1b shows an illustration of the molecule force interactions in the oil and at the interface between oil and water. This molecular force contraction per unit length is defined as the interface tension (Schwartzstein et al. 2005). Within a liquid the molecule will be surrounded on all sides by

other similar molecules that exert force on it, but because of the molecular arrangement symmetry there is no net molecular movement. However at the interface between oil and water, the liquid which is much "stronger" will dominate the interface. In the example of oil and water, the water is denser and therefore has higher wettability strength and will occupy a larger area on the solid than oil. The oil phase will contract itself to the smallest possible area. You may then ask yourself what is keeping the oil from contracting and then collapsing. This can be explained by the Laplace law which is given in equation (2.1). The equation gives the interfacial tension between the two liquids as a function of capillary pressure. Capillary pressure is expressed as the pressure discontinuity that is generated at any point on the interface between the nonwetting and wetting phase (Bear et al. 1991). In equilibrium the expression for the capillary pressure is given by the Laplace eqation as following (Bear et al. 1991),

$$P_c = P_c(S_w) = P_{nw}(S_w) - P_w(S_w) = \sigma_{f_{nw},f_w} \left( \frac{1}{r_{nw}} + \frac{1}{r_w} \right) \tag{2.1}$$

where $S_w$ is the saturation of the wetting fluid, $\sigma_{f_{nw},f_w}$ is the interfacial tension between the nonwetting and wetting fluid, $P_w$ and $P_{nw}$. is the pressure in the wetting and nonwetting fluid, respectively. $r_{nw}$ and $r_w$ are the principal radii of the curvature at the interface which are not usually measured. Mean radius of curvature, $r_m$, is used and equation (2.1) can be rewritten as following,

$$P_c = \frac{2\sigma_{f_{nw},f_w}}{r_m} \tag{2.2}$$

The pressure discontinuity that arises can be explained by the fact that the oil does not collapse, but exerts a capillary pressure on the water. It can be visualized by considering an oil sphere which is surrounded by water. Although water is denser and oil would want to contract to smallest possible area, it will stop its contraction at a certain point. At this point the capillary pressure is the pressure "inside" the sphere. The smaller the radius of the sphere the larger the capillary pressure will be. Therefore in order to maintain a porous medium partially saturated with a nonwetting fluid and a wetting fluid the pressure of the nonwetting fluid has to be a value greater than that of the wetting fluid (Ahmed et al. 2010). The pressure excess in the nonwetting fluid is the capillary pressure, and this quantity is a function of the wetting phase saturation (Tarek et al. 2010). Saturation can be defined as the fraction of a

fluid in a given pore space. Water saturation can be calculated by equation (2.3) if we consider only oil and water in the pore space.

$$S_w = \frac{V_v - V_o}{V_v} \tag{2.3}$$

where $V_v$ is the volume of the void space and $V_o$ is the volume of oil in the pore space. Since it is only considered to be oil and water in the pore space the saturation of oil is equal to $S_o = 1 - S_w$. Finally the capillary pressure for oil and water interactions can be expressed by equation (2.4).

$$P_c(S_w) = P_o(S_w) - P_w(S_w) \tag{2.4}$$

Figure 2.2 shows a typical capillary pressure curve for a core sample where water is the wetting phase and oil is the nonwetting phase. The $P_c(S_w)$ curve for increasing $S_w$ is called imbibition curves, while capillary pressure curve for decreasing $S_w$ are called drainage curves (Barenblatt et al. 1990). In other words the drainage process is when oil displaces water, and imbibition process is when water discplaces oil. Imbibition is the reverse action of drainage and is the flow process of interest in oil reservoir migration (Ahmed et al. 2009).
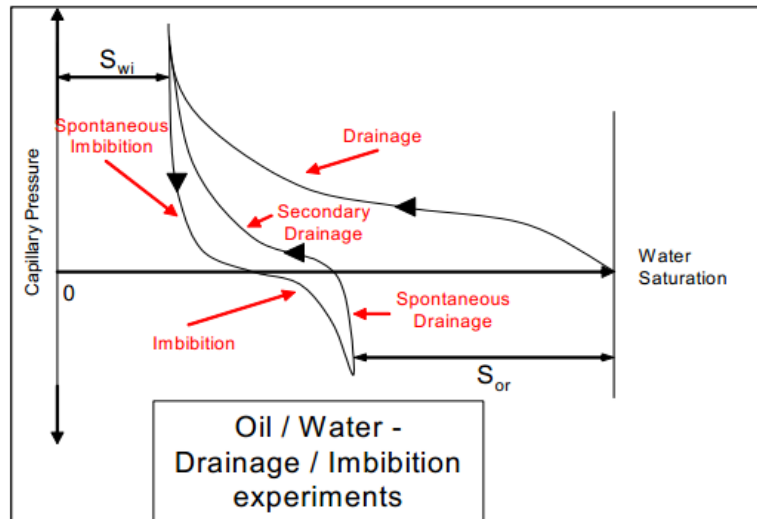


*Figure 2.2: Example of the capillary pressure curve for oil and water system. Courtesy of Vinci Technologies.*

However one would assume that the drainage curve and the imbition curve would fall perfectly on the same line, but that is not the case in real porous media due to *hysteresis*. Hysteresis is a term to explain the process of fluid entrapment. Capillary hysteresis is a result of several factors, to mention a few pore geometry, fluid configurations and chemical

interactions. The pore interconnectivity can hinder the movement of fluid phases and result in irreducible saturation for the water and oil phase. In the subsequent sections the cause to capillary hysteresis is explained combined with typical phase entrapment which is implemented in the simulation.

### 2.1.1 Contact angle hysteresis

As mentioned before the wetting characteristics of the fluid play an important role in the rise or decrease of the capillary pressure. The ability a fluid phase has to wet a solid surface when in presence of a second immiscible fluid phase is called wettability (Fanchi et al. 2005). The intermolecular interactions that occur when a liquid contacts a solid surface can cause the liquid to either spread into a thin film or shrink to minimize its contact area (Asthana et al. 2006). Whether the liquid will spread out or shrink depends on the strength of wettability. The strength of wettability is measured by the *contact angle*. The contact angle is always measured through the denser phase and is related to interfacial energies by

$$\sigma_{os} - \sigma_{ws} = \sigma_{ow} \cos \theta \tag{2.5}$$

where $\sigma_{os}$ is the interfacial energy between oil and solid, $\sigma_{sw}$, is the interfacial energy between solid and water and $\sigma_{ow}$ is the interfacial energy between oil and water. $\theta$ is the contact angle between the two fluids. By earranging equation (2.5) we get the following expression for the interfacial energy between oil and water.

$$\sigma_{ow} = \frac{\sigma_{os} - \sigma_{ws}}{\cos \theta} \tag{2.6}$$

Equation (2.6) indicates that if the contact angle decreases the interfacial tension between oil and water will increase. Increasing the interfacial tension will result in a higher capillary pressure as indicated in equation (2.2).
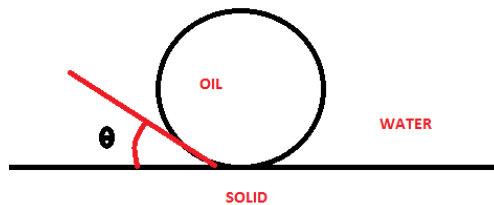


*Figure 2.3: Illustrative of wettability of oil and water.*

Figure 2.3 shows an illustration of the strength measurement of the contact angle, and as depicted in the figure the smaller the contact angle the stronger the wettability is for the water

phase. The important characteristic of solid-liquid and liquid-liquid interface interactions is *contact angle hysteresis*. Contact angle hysteresis is governed by adhesion, surface roughness and heterogeneity of the two phases which are in contact (Bhusan et al. 2011). The energy required to separate any two substances will always be greater than the energy gained by bringing them together. This loading and unloading cycle is a thermodynamically irreversible loss of energy process, and is refered as capillary hysteresis. As shown in figure 2.2 the capillary pressure during imbibition is lower than during the drainage process due to the loss of energy. The process of saturating or desaturating the porous media with the nonwetting phase is one of two causes for contact angle hysteresis (Ahmed et al. 2009). The other cause is the varation of the pore channel section area (Barenblatt et al. 1990). Contact angle hysteresis can be grouped into either thermodynamic or kinetic hysteresis. Thermodynamic contact angle hysteresis is a function of the surface roughness and heterogenity of the pore channel. While kinetic contact angle hyteresis describes the hysteresis produced when the contact angle is changed with time due to kinetic changes in the system. The contact angle hysteresis will give result to a difference of events depending on whether drainage or imbibition occurs. For the drainage processes events such as Haines jump will occur, and for imbibitio processes piston like invasion and snap off can occur. All events are explained in the following sections.

### 2.1.2 Haines jump

During the drainage process the porous media will get more saturated with the nonwetting fluid. The capillary pressure will increase in accordance with equation (2.3), and the pressure of the nonwetting phase increases as the saturation of the nonwetting fluid rises. As explained in detail in previous chapter, the Laplace law concludes that increasing the capillary pressure will result in a higher radius of curvature or alteration in the surface tension of the fluids. Assuming the surface tension stays the same, the nonwetting phase will expand creating a critical interface. The critical interface is defined as the critical curvature and is the last stable curvature before the invading fluid occupies the entire pore space (Prodanovic et al. 2006b). The nonwetting phase will cause an abrupt movement of the interface, a so-called Haines Jump (Lenordmand et al. 1983). The jumps occur over a small timescale and the rules that govern the movement are based on the calculations of stability of the interfaces (Lenordmand et al. 1983). Figure 2.4 shows an illustration of a Haines jump. As shown in the figure the oil phase will have an abrupt movement, causing a large amount of oil phase filling in the pore space. It will stop when the oil phase encounters a pore throat that is smaller than the pore throat it "broke through".
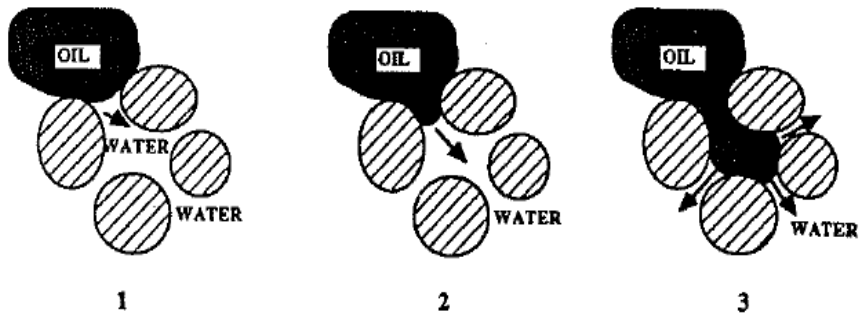
*Figure 2.4: Haines jump in pore throat for drainage events (Jerauld et al. 1990).*

### 2.1.3 Piston like invasion

Haines jump occur during the drainage process, for imbibition processes experiments have shown two different mechanisms that dominate, the piston like invasion and the snap off. Imbibition is in our simulation and as mentioned before is the process of invading the pore body with the wetting fluid i.e. invading the pore body with water. It is important to note that in the imbibition process the wetting phase will preferably imbibe into smaller pore bodies and throats (Barrera et al. 2007). In piston like invasion the pore body can be invaded by the wetting phase at a particular capillary pressure value, only if the apparent size is lower than the critical value that is required to balance the current capillary pressure (Barrera et al. 2007). Furthermore experiments have shown that the probability of invasion of a pore body by the wetting fluid (water) will decrease with the number of connected pore throats that are filled with the nonwetting phase (oil) (Barrera et al. 2007). Hence the apparent size of a pore body is a function of the radius and number of throats containing the nonwetting fluid.
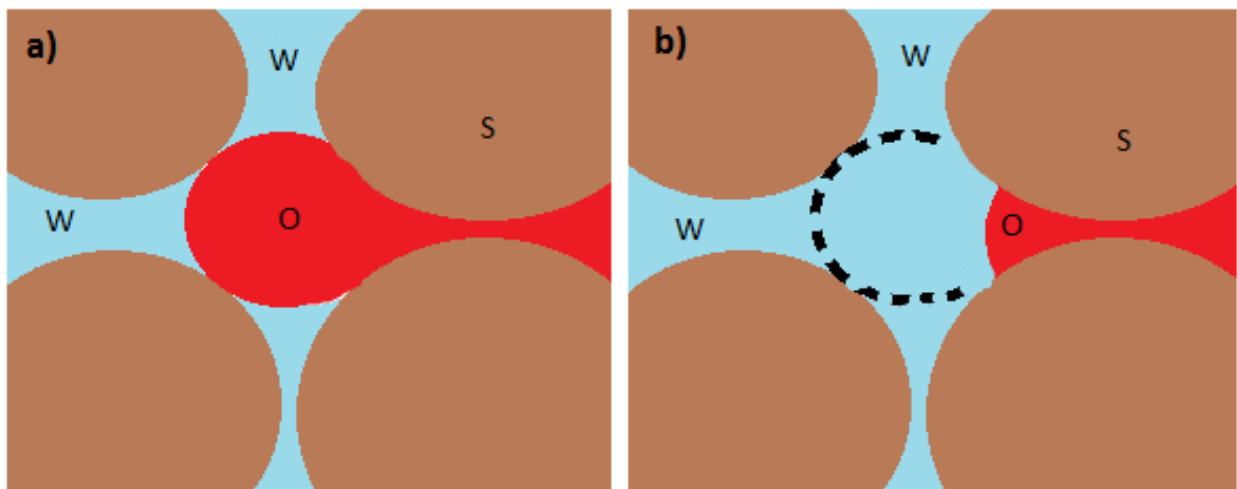


*Figure 2.5: Piston like invasion in a pore throat for imbibition events.*

Therefore as long as the number of throats containing oil and the radius is lower than the critical value the piston like invasion will take place. As shown in figure 2.5 the water will push oil further in the pore throat and the interface is still present at the end of the throat. Piston like invasion will occur at a more favorable pressure than snap off. Snap off occurs only when the piston like invasion is topologically impossible due to pore interconnectivity. In the following section a description of snap off is elaborated.

### 2.1.4 Snap off

Snap off is a process that occurs during imbibition (Jerauld et al. 1990). In a snap off process the nonwetting phase will exhibit a saddle-shaped interface. This is due to the fact that the decrease in capillary pressure will result in oil contracting to the smallest possible area before it will snap off and separate completely.
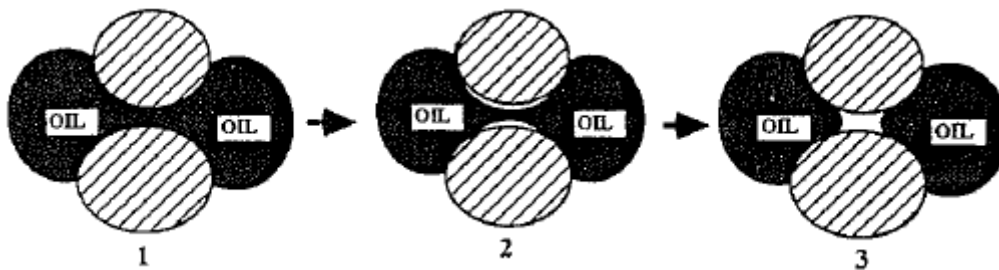


*Figure 2.6: Snap off in pore throat for imbibition events (Jerauld et al. 1990).*

This mechanism can be explained by the discontinuity in pressure over the interface. Because the capillary pressure will decrease, it will make the wetting phase "stronger" and therefore it will occupy a larger surface area. This higher pressure in the wetting fluid combined with the small size of the pore throat causes suction in the wetting fluid from adjacent throats (Barrera et al. 2007). The suction is explained as a transport of the wetting fluid from the edges of the pore body into the edges of the throat, with a tendency toward equalizing the capillary pressure (Vaifai et al. 2009). Illustration of the mechanism and saddle-shaped interface split is shown in figure 2.6.

All the mechanism and characteristics of the capillary pressure change and curvature change is implemented in the level set method. However the level set method is not the only method used to describe the capillary pressure, saturation and interfacial relationship. The following chapter gives a short description of other methods used in this area.

## 2.2 Pore scale modeling techniques

The classical macro-scale models to represent the multiphase flow rely heavily on the Navier-Stokes equation and the extensions of Darcy's law (Porter et al. 2009). A model of macroscopic scale does not capture the important physical phenomena of multiphase flow such as the fluid-fluid interfaces, because the capillary pressure is assumed to be a function of $S_w$ only (Porter et al. 2009). The classical macro-scale models to represent the multiphase flow rely heavily on the Navier-Stokes equation and the extensions of Darcy's law (Porter et al. 2009). A model of macroscopic scale does not capture the important physical phenomena of multiphase flow such as the fluid-fluid interfaces, because the capillary pressure is assumed to be a function of $S_w$ only (Porter et al. 2009). A numerous models have been proposed to give an accurate microscopic description of the capillary pressure, saturation and interfacial area relationship for a porous media. These include the pore network model, Lattice-Boltzmann model and the main topic of this thesis which is the level set model. The level set method will be explained in detail in the subsequent chapter.

### 2.2.1 Lattice-Boltzmann model

The more general definition of the lattice Boltzmann method (LBM) is that it is a method to bridge the gap between micro-scale and macro-scale by not considering each particle behavior alone, but the behavior of a collection of particles as a unit (Mohamad et al. 2011). The unit of particles is represented by a distribution function (See figure 1b). In the work done by Porter et al. 2009 a multiphase lattice Boltzmann simulation is used to investigate the hysteresis in a glass bead porous system. The simulation conducted drainage and imbibition simulation of the porous system. The LB model studies the relationship between the capillary pressure, wetting phase saturation and nonwetting-wetting interfacial area per volume. The result showed that the model gave good agreement of experimental data by Culligan et al. 2004 for drainage, but was less satisfactory for imbibition.

### 2.2.2 Pore network model

The pore network method is an idea to map the porous medium onto equivalent network of interconnected pore throats and pore bodies (Muhammad et al. 2011). Exact mapping of the pore space onto an equivalent pore network has proven to be difficult. The porous media is very heterogeneous and the mapping of the interconnected pore throats and bodies involves a judicious choice of what constitutes a pore throat or pore body, and where they are connected (Muhammad et al. 2011). The development of a pore network model needs three

characteristics measured. These characteristics are the pore size, pore length and the average connectivity of the porous media. When these properties have been found through techniques which will not be introduced here, the next step is selecting a shape for the pore throats. The choice may be cylindrical or slit-like, or have converging-diverging segments.

The model proposed by Joekar-Niasar et al. 2009 determines the pore geometry by means of a pore network model. The network model gives a simulated set of drainage and imbibition experiments performed on a two-dimensional micromodel (Joekar-Niasar et al. 2009). The models approach for constructing the pore geometry is to find the medial axis by a pixel-based distance transform. Their analysis showed encouraging results, and they presented a good predictive tool from the pore network model for the relationship between the capillary pressure, water saturation and fluid-fluid interfacial area.
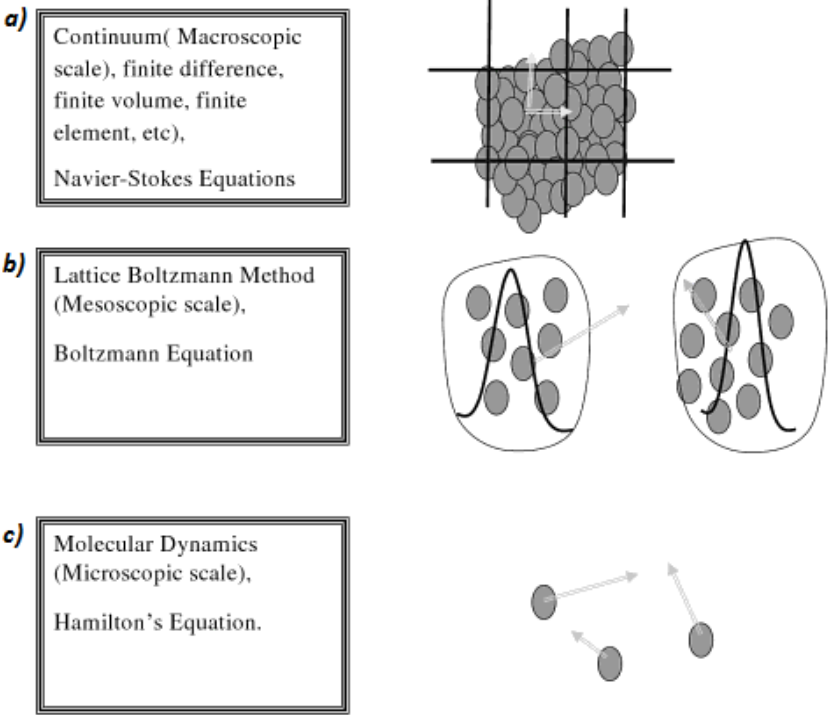


*Figure 2.7: Schematic illustration of the different techniques used for simulation. a) Macroscopic scale b) Mesoscopic scale c) Microscopic scale (Mohamad et al. 2011).*

# CHAPTER 3

# THE LEVEL SET MODEL

The following chapter gives a short description of the applied mathematics used to develop the level set model.

## 3.1 The level set method

The level set method was developed by Osher and Sethian (1988) and is a tool that can describe the exact position and shape of the fluid and solid interfaces in realistic fracture geometry (Prodanovic et al. 2008). In other words it is a numerical method for propagating interfaces (Prodanovic et al. 2012)
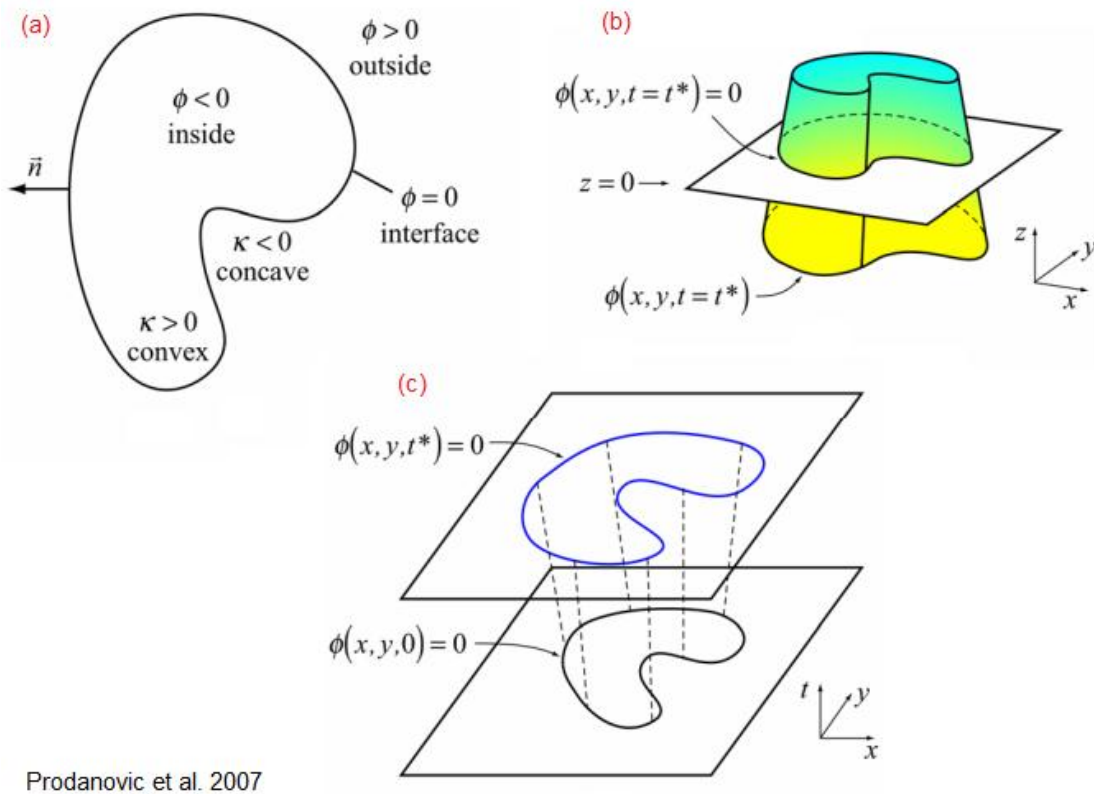


*Figure 3.1: a) Illustrative 1D interface (closed surface) for the zero level set ($\varphi = 0$) of a real valued level set function $\varphi$, which is defined over the entire 2D domain. b) How the level set in a) is obtained. c) Different locations of the interface at time $t^*$, where $t^* = 0$ represents its initial location.*

The method describes the interface evolution implicitly by a function $\varphi(x, y, t)$ which is a dimension higher than the interface. The method consists of letting the interface between the two predefined phases to be described by the zero level set, which is the set of points $\vec{x}$ that satisfy $\varphi(x, y, t) = 0$ (See figure 3.1a). Furthermore the sign of $\varphi(x, y, t)$ determine the interior and exterior of the interface boundary (See figure 3.1). The topological interface changes such as merging and splitting are handled naturally. As depicted in figure 3.1a) depending on the users predefined sign for the interior and exterior, the level set for our simulation will have the same notation as the one in the figure. If the implicit function gives a value which is larger than zero it will be outside the interface and inside the interface when the function is less than zero. In the level set method developed by Helland et al. [2011} at IRIS, the implicit function will be larger than zero in the wetting phase and less than zero for the non-wetting phase, and equal to zero at the interface between the two fluids. Similar description for the interface between void and solid is also implemented in the simulation. Table A.1 in the appendix gives a description of the signs the implicit functions calculates in the simulation for the different interfaces. In order to fully understand the level set method, the implicit function $\varphi$ has to be explained and is done so briefly in the following sections.

## 3.2 Signed distance function

Till now it has been explained that an implicit function $\varphi$ has to be used to determine the interface between fluid-fluid contact and solid-void contact. The properties of an implicit function serve well for the level set method compared to an explicit representation. The benefits of implicit representation is that the interface can be represented as the isocontour of the function $\varphi$. Hence the implicit function $\varphi$ needs to be chosen in such a way that its zero isocontour can be used to represent the surface of interest. The function has to be zero at the interface, negative in the interior and positive in the exterior as mentioned in previous chapters. Firstly we look at the distance function $d(\vec{x})$ which can be defined as following,

$$d(\vec{x}) = \min(|\vec{x} - \vec{x}_I|) \text{ for all } \vec{x}_I \in \partial\Omega \tag{3.1}$$

where $\partial\Omega$ represents the interface and $\vec{x}_I$ is the position vector at the interface. Furthermore $|\nabla d| = 1$, this is an important property to be noted. The basic concept of the distance function and its properties are implemented in the *signed distance function*. The properties are listed below.

1. $|\varphi(\vec{x})| = d(\vec{x})$ for all $\vec{x}$

2. $\varphi(\vec{x}) = d(\vec{x}) = 0$ for all $\vec{x} \in \partial\Omega$

3. $\varphi(\vec{x}) = -d(\vec{x})$ for all $\vec{x} \in \Omega^-$

4. $\varphi(\vec{x}) = d(\vec{x})$ for all $\vec{x} \in \Omega^+$

where $\Omega^+$ represents the exterior and $\Omega^-$ represents the interior. And last but not least the signed distance function satisfies the following equation:

$$|\nabla\varphi| = 1 \tag{3.2}$$

This property is a natural choice for $\varphi(x, t)$ due to numerical stability obtained because $\nabla\varphi$ is neither very flat nor very steep. Furthermore the void-solid signed distance function, $\varphi_{vs}$, is computed by the *reinitialization equation* given in equation (3.3).

$$\varphi_t + S(\varphi)(|\nabla\varphi| - 1) = 0 \tag{3.3}$$

where $S(\varphi)$ is a sign function that is continually updated as calculations progress. The numerical approximation for $S(\varphi)$ is given in equation (3.4).

$$S(\varphi) = \frac{\varphi}{\sqrt{\varphi^2 + |\nabla\varphi|^2(\Delta x)^2}} \tag{3.4}$$

Equation (3.4) is also updated continually as the calculation progresses so that the term $|\nabla\varphi|$ gives the intended effect on the simulations. The reinitialization procedure is used to compute the fluid-fluid signed distance function, denoted as $\varphi_{ow}$, based on an input fluid configuration file (Helland et al. 2011). The input file is a micro CT scan of a real porous media. The input files are explained in further detail in chapter 4. For each capillary pressure the signed distance function $\varphi_{ow}$ is evolved until it reaches steady state. Steady state is reached when the *Level set equation* is solved.

## 3.3 The Level Set Equation

The level set value of a particle on the front with path $\vec{x}(t)$ will be equal to zero $(\varphi(\vec{x}(t), t) = 0)$ also shown in figure 3.1. Furthermore by using the chain rule the zero level set equation can be rewritten as following,

$$\frac{\partial\varphi}{\partial t} + \nabla\varphi \frac{d\vec{x}(t)}{dt} = 0 \tag{3.5}$$

The first term is later denoted as $\varphi_t$ and the second term gives the gradient of the implicit function ($\nabla\varphi$) and the velocity of the particle path. The velocity of the particle will have a component in the normal direction and one in the tangential direction as shown equation (3.6).

$$\frac{d\vec{x}(t)}{dt} = \vec{V} = V_n\vec{N} + V_t\vec{T} \tag{3.6}$$

Where $\vec{T}$ and $\vec{N}$ denotes the tangent and normal vector, respectively. As shown in figure 3.1a the vector $\vec{N}$ points normally to the level sets and since $\vec{N}$ and $\nabla\varphi$ point in the same direction and $\vec{T}$ is orthogonally on $\vec{N}$, $\vec{T} \cdot \nabla\varphi = 0$ for any tangent vector. Therefore the level set equation

$$\varphi_t + \left(V_n\vec{N} + V_t\vec{T}\right) \cdot |\nabla\varphi| = 0 \tag{3.7}$$

is equivalent to

$$\varphi_t + V_n\vec{N} \cdot |\nabla\varphi| = 0 \tag{3.8}$$

Furthermore the local unit normal to the interface is given in equation (3.9)

$$\vec{N} = \frac{\nabla\varphi}{|\nabla\varphi|} \tag{3.9}$$

As a result of,

$$\vec{N} \cdot \nabla\varphi = \frac{\nabla\varphi}{|\nabla\varphi|} \cdot \nabla\varphi = \frac{|\nabla\varphi|^2}{|\nabla\varphi|} = |\nabla\varphi| \tag{3.10}$$

we may rewrite equation (3.5) as

$$\varphi_t + V_n|\nabla\varphi| = 0 \tag{3.11}$$

The level set model developed by Helland et al.[ 2011] has an interface motion which depends directly on the level set function $\varphi(\vec{x}(t), t)$ and has motion by mean curvature where the interface moves in the normal direction. Motion by mean curvature contains only a component in the normal direction, i.e., the tangential component is identically zero as mentioned before. Therefore the term $V_n$ in equation (3.11) is the speed of the interface in direction normal to itself. The speed of the interface, $V_n$, represents the balance between the capillary and interfacial forces as following:

$$V_n = \vec{V} \cdot \vec{N} = C - \kappa \tag{3.12}$$

where $C = P_c/\sigma$ is the input interfacial curvature and $\kappa$ is the mean curvature of the interface (Helland et al. 2011). The level set for our application can finally be written as following,

$$\varphi_t + (C - \kappa)|\nabla\varphi| = 0 \tag{3.13}$$

In the above equation the $|\nabla\varphi|$ term is solved by discretizing it using the Hamilton-Jacobi Weighted Essentially Non-Oscillatory technique (HJ WENO) and Godunov's method. The mean curvature is solved by the central difference formulas, all methods are described in subsequent sections.

## 3.4 Numerical Discretization

In the following sections the discretization methods are explained. All methods give approximations to the calculations in the simulation.

### 3.4.1 HJ WENO and Godunov's method for upwinding.

To be able to evolve and move the equation $\varphi$ forward in time across a predefined grid, a method called *upwind differencing* is used. At time $t^n$ the current value of the implicit function can be defined as $\varphi^n = \varphi(t^n)$. After every time increment $\Delta t$ the implicit function needs be updated for every grid point. The new values can be represented as $\varphi^{n+1} = \varphi(t^{n+1})$, where $t^{n+1} = t + \Delta t$. A simple first-order accurate method for time discretization given by the forward Euler method,

$$\frac{\varphi^{n+1} - \varphi^n}{\Delta t} + \vec{V}^n \cdot \nabla\varphi^n = 0 \tag{3.14}$$

where $\vec{V}^n$ is the velocity of the implicit function at time $t^n$, and $\nabla\varphi^n$ is the gradient operator at time $t^n$ for the implicit function. Expanding the above equation the following is obtained,

$$\frac{\varphi^{n+1} - \varphi^n}{\Delta t} + u^n\varphi_x^n + v^n\varphi_y^n + w^n\varphi_z^n = 0 \tag{3.15}$$

The sign of $u, v$ and $w$ determine whether the values of $\varphi$ are moving to the right or left of its respective coordinate direction. This can be explained by considering a point $x_i$, where the spatial derivative of $\varphi$ is denoted as $(\varphi_x)_i$. Equation (3.15) can then be written as,

$$\frac{\varphi_i^{n+1} - \varphi_i^n}{\Delta t} + u_i^n(\varphi_x)_i^n = 0 \tag{3.16}$$

Using the *method of characteristics* if $u$ at a grid point $i$ is positive, the values of $\varphi$ are moving to the right. And to determine the value of $\varphi$ we have to look to the left of the grid point position $x_i$. This partial derivative is denoted as $\varphi_x^-$ If on the other hand the velocity u is negative, the implicit function at that grid point is moving from right to left. The method of characteristics tells us to look to the right of $x_i$ to determine an appropriate value of $\varphi_i$ at time $t^{n+1}$. This partial derivative is denoted as $\varphi_x^+$. The method of choosing an approximation to the spatial derivate based on the sign of u is known as *upwinding*. Generally, upwinding approximates derivatives by biasing the finite difference stencil in the direction where the characteristics information is coming from (Osher et al. 2003). Furthermore to obtain an accurate calculation of $\varphi_x^-$ and $\varphi_x^+$ the Hamilton Jacobi Weighted Essentially Nonoscillatory (HJ WENO) polynomial interpolation is used. A detailed mathematical approach will not be shown here but can be found in many applied mathematical books, reader is advised to refer to Osher et al [2003] for more detailed description. The basic idea of Hamilton Jacobi Essentially Nonoscillatory (HJ ENO) polynomial interpolation is that it is a method which allows one to extend the first order accurate upwinding, which was explained earlier, to higher-order spatial accuracy giving better approximations to $\varphi_x^-$ and $\varphi_x^+$. This is done by using the smoothest possible polynomial interpolation to find $\varphi$ then differentiating to get $\varphi_x$. A number of mathemathical steps will result in exactly three possible HJ ENO approximations for $\varphi_x^-$. These three approximations can be found in the appendix. Furthermore this is where the HJ WENO method is included, and is an approach to give an even better approximation of $\varphi_{\bar{x}}$. This is because the HJ WENO method takes a convex combination of the three ENO approximations, and if any of the three approximations interpolates across a discontinuity it will be given the minimal weight. This minimizes its contribution and the total error of the simulation, because picking only one of the three stencils as done with the HJ ENO method is will give a bad approximation in smooth regions where the data is well behaved (Osher et al. 2003).

Furthermore the Godunov's method for upwinding is used to determine $\varphi_x, \varphi_y$ and $\varphi_z$ from the result obtained by the HJ WENO method. Thus the Godunov's method determines which result of $\varphi_x^-$ and $\varphi_x^+$ will be used to determine $\varphi_x$. The same goes for $\varphi_y$ and $\varphi_z$. The Godunov's method is a good method for avoiding artificial dissipation because it chooses the most meaningful solution (Osher et al. 2003). The elegant formula by Rouy and Tourin is implemented in the model and has the following form for $C > 0$ (Osher et al. 2003),

$$\varphi_x^2 \approx max\big(max(\varphi_x^-, 0)^2, min((\varphi_x^+, 0)^2)\big) \tag{3.17}$$

and for $C < 0$,

$$\varphi_x^2 \approx max\big(min(\varphi_x^-, 0)^2, max((\varphi_x^+, 0)^2)\big) \tag{3.18}$$

### 3.4.2 Central Differences

As shown in figure 3.1 the zero level set is a one-dimensional interface between a two-dimensional non-circular object at an instant at time, and the curvature $\kappa$ of the interface varies with location (Figure 3.1a). If the curvature $\kappa$ is larger than zero the curve will have a convex shape, and if it is less than zero it will have a concave shape (see figure 3.1a). The mean curvature of the interface is defined as the divergence of the normal $\vec{N} = (n_1, n_2, n_3)$ (Osher et al. 2003),

$$\kappa = \nabla \cdot \vec{N} \tag{3.19}$$

where $\nabla\varphi = (\varphi_x, \varphi_y, \varphi_z)$ is the spatial gradient of $\varphi$. Inserting equation (3.9) into (3.14) will give the following equation for the curvature of each level set,

$$\kappa = \left( \begin{matrix} \varphi_x^2\varphi_{yy} - 2\varphi_x\varphi_y\varphi_{xy} + \varphi_y^2\varphi_{xx} + \varphi_x^2\varphi_{zz} - 2\varphi_x\varphi_z\varphi_{xz} + \varphi_z^2\varphi_{xx} \\ -2\varphi_y\varphi_z\varphi_{yz} + \varphi_z^2\varphi_{yy} \end{matrix} \right) \Big/ |\nabla\varphi|^3 \tag{3.20}$$

The $\kappa$ term is solved by the central difference formulas given in appendix A.2, which are used to discretize the spatial derivatives of $\phi$ in the curvature term given in equation (3.20).The equations given in appendix A.2 are only approximations to the spatial derivatives.

### 3.4.3 Time update

To advance the front forward in time, a method for the time discretization has to be implemented in the model. The time update in the model is done by using the TVD RK method, and the adaptive time stepping based on the CFL condition.

As mentioned before the HJ WENO allows us to discretize the spatial term in the level set equation to fifth order accuracy. The level set method is quite sensitive to spatial accuracy and therefore the fifth order accuracy of the HJ WENO method is the best choice. If the temporal truncation error is less likely to get progressively large, it may be concluded that the forward Euler time discretization is usable for time discretization (Osher et al. 2003). However the forward Euler time discretization in equation (3.14) gives only first-order accuracy in time

and it is known for a fact that the error for our simulation will increase when invasion for larger and larger pore throats occur. Therefore higher order temporal discretization is needed in times when it is necessary to obtain a more accurate numerical solution. In the level set model the total variation diminishing (TVD) Runge-Kutta (RK) method is used for temporal discretization. This method increases its accuracy by the *method of lines* approach. The method of lines approach allows the temporal discretization of the partial differential equation to be treated as an ordinary differential equation. This is done in a semidiscrete manner where the spatial discretization is separated from the temporal discretization.

Basic first order accurate TVD RK is the first step in forward Euler method. The third order accurate TVD RK scheme takes first an Euler step to advance the solution to time $t^n + \Delta t$,

$$\frac{\varphi^{n+1} - \varphi^n}{\Delta t} + \vec{V}^n \cdot \nabla \varphi^n = 0 \tag{3.21}$$

then the second Euler step to advance the solution to time $t^n + 2\Delta t$,

$$\frac{\varphi^{n+2} - \varphi^{n+1}}{\Delta t} + \vec{V}^{n+1} \cdot \nabla \varphi^{n+1} = 0 \tag{3.22}$$

followed by an averaging step

$$\varphi^{n+\frac{1}{2}} = \frac{3}{4} \varphi^n + \frac{1}{4} \varphi^{n+2} \tag{3.23}$$

Equation (3.23) produces an approximation to $\varphi$ at time $t^n + \frac{1}{2}\Delta t$. Furthermore another Euler step is taken to advance the solution to time $t^n + \frac{3}{2}\Delta t$ which is also followed by an averaging step. Combining the TVD RK scheme with central differencing for the spatial discretization will result in a stable numerical method for time discretization. In our model when we solve for stable fluid configurations the error will not become less as we advance in time. The reason for this is because the interfacial area sometimes will penetrate through larger pores, and when penetrating larger pores the error will increase. Likewise the error will decrease when the pores become narrower and till stabile configuration is achieved. Hence if we are looking at a static problem, for example when the signed distance function is reinitialized, the error will get less for every iteration step. For a static problem as during the reinitialization process the TVD method is the one to be used for time discretization. But for the problem mentioned above, when the penetration happens in pore throats that increase in size the Courant-Friedreich-Levy (CFL) condition needs to be applied. This is because this condition decides how large the time step for the numerical method used to solve equation (3.14) can

get for numerical stability and convergence against the right solution. Once all terms have been discretized, and the TVD RK method has been used to advance the front in time (Osher et al. 2003). The adaptive time stepping based on CFL condition is applied. The equation implemented in the level set code for the time restriction is given in equation (3.24) (Osher et al. 2003).

$$\Delta t \left( \frac{|H_1|}{\Delta x} + \frac{|H_2|}{\Delta y} + \frac{|H_3|}{\Delta z} + \frac{2a}{(\Delta x)^2} + \frac{2a}{(\Delta y)^2} + \frac{2a}{(\Delta z)^2} \right) < 1 \tag{3.24}$$

$a$ is a the curvature constant, which is equal to 1 in our simulation. $H_1$, $H_2$ and $H_3$ are the Hamilton-Jacobi equations for each direction. For our simulation $H_1$ is equivalent to $C\varphi_x$ etc., also for our simulation $\Delta x = \Delta y = \Delta z$. Implementing these changes the CFL condition used in the level set code is given in equation (3.25) below.

$$\Delta t \left( \frac{|C\varphi_x| + |C\varphi_y| + |C\varphi_z|}{\Delta x |\nabla \varphi|} + \frac{6}{(\Delta x)^2} \right) < \alpha \tag{3.25}$$

Rewritten for simplification,

$$\Delta t < \frac{\alpha}{CFL} \tag{3.26}$$

where $\alpha = 0.5$ in our model.

Much of the purpose of this thesis is to investigate interfacial area between oil and water and its effect on hysteresis. The following sub chapter gives a short description of the volume and surface integral, which is used to calculate the interfacial area between oil and water.

## 3.5 Volume and surface integral

Saturation and interfacial areas are calculated at each steady state by volume and surface integrals. The volume integral for the non-wetting fluid can be calculated by the following equation,

$$V_o = \int_\Omega H(-\varphi) d\vec{x} \tag{3.27}$$

Furthermore the surface integral given in equation (3.28) can be used to calculate the interfacial area between any fluid-fluid interactions.

$$A_{f-f} = \int_\Omega \delta\big(\varphi(\vec{x})\big)|\nabla\varphi(\vec{x})|d\vec{x} \tag{3.28}$$

The above equation can be rewritten to represent the interfacial area between oil and water, where water is the wetting phase,

$$A_{ow,tot} = \int_\Omega \delta(\varphi_{ow})|\nabla\varphi_{ow}| \cdot dx \tag{3.29}$$

The procedure to find only the point contacts between oil and water involves the calculation of the *Heaviside* and *Dirac delta* functions. Furthermore by implementing the Heaviside function and Dirac Delta function in equation (3.29), the equation given below is the interfacial area between oil and water excluding the thin film on the solid wall.

$$A_{ow} = \int_\Omega H(-\varphi_{vs} - b \cdot \Delta x)\delta(\varphi_{ow})|\nabla\varphi_{ow}| \cdot dx \tag{3.30}$$

The above equation includes a few symbols which have not been explained yet. Such as the Heaviside function $H$, the Dirac delta function $\delta$ and the b factor. The Heaviside function is a step function which is defined to be equal to zero for every negative value of $\varphi$ and to unity for every positive value of $\varphi$ and we may write the following (Osher et al. 2003),

$$H(\varphi) = \begin{cases} 0 & if\ \varphi\ \leq 0 \\ 1 & if\ \varphi\ > 0 \end{cases}$$

where $\varphi$ is the signed distance function which is a function of the multi-dimensional variable $\vec{x}$. Because the variable $\vec{x}$ is of multi-dimensional order the Heaviside function is defined as a function of $\varphi$ for simplicity (Osher et al. 2003). Derivation of the one-dimensional Heaviside function gives us the Dirac delta function as shown in equation (3.31).

$$\delta(\varphi) = H'(\varphi) \tag{3.31}$$

To avoid the discontinuity at $\varphi(x = 0)$ in the numerical calculations we use a smeared out version of the Heaviside function (Osher et al. 2003). This is done by selecting a tolerance value $\varepsilon$ whose value if of the order of the width of the numerical cell, such that (Prodanovic et al. 2012):

$$H(\varphi) = \begin{cases} 0 & \varphi < -\varepsilon \\ \dfrac{1}{2} + \dfrac{\varphi}{2\varepsilon} + \dfrac{1}{2\pi} \sin\left(\dfrac{\pi\varphi}{\varepsilon}\right) & -\varepsilon \leq \varphi \leq \varepsilon \\ 1 & \varphi < \varepsilon \end{cases} \tag{3.32}$$

According to Osher et al. [2003] the best value for the tolerance is $\varepsilon = 1.5$, and is the value implemented in our simulations as well. Furthermore the Dirac delta function is as mentioned before the derivative of the Heaviside function and is given in equation (3.33).

$$\delta(\varphi) = \begin{cases} 0 & \varphi < -\varepsilon \\ \dfrac{1}{2\varepsilon} + \dfrac{1}{2\varepsilon} \cos\left(\dfrac{\pi\varphi}{\varepsilon}\right) & -\varepsilon \leq \varphi \leq \varepsilon \\ 0 & \varphi < \varepsilon \end{cases} \tag{3.33}$$

The smeared Heaviside function and the Dirac delta function from equation (3.30) and (3.31) are illustrated in figure 3.2.
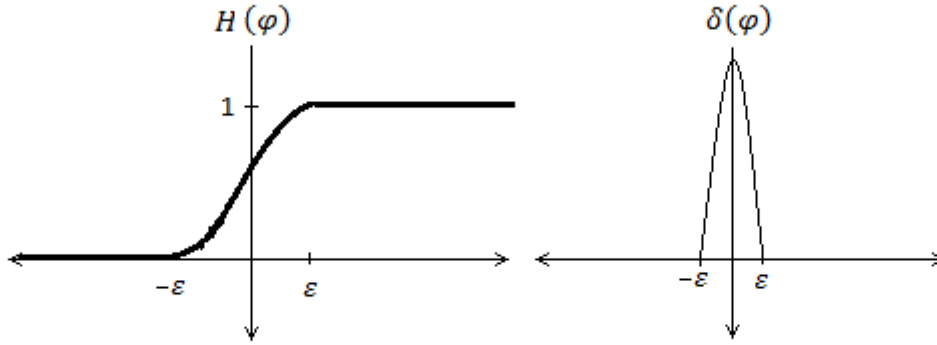


*Figure 3.2: Illustration of the smeared out Heaviside function and its derivative.*

Figure 3.2 shows a general illustration of the Heaviside function and its corresponding delta function. In our simulation we would like to not account for the interfacial which is the thin film on the solid wall. In order to do so the b-factor is introduced. The Heaviside function will have the following form,

$$H(-\varphi_{vs} - b \cdot \Delta x)$$

$$= \begin{cases} 0 & \varphi_{vs} > \varepsilon - b \cdot \Delta x \\ \dfrac{1}{2} - \dfrac{\varphi_{vs}}{2\varepsilon} - \dfrac{b \cdot \Delta x}{2\varepsilon} + \dfrac{1}{2\pi} \sin\left(\dfrac{\pi}{\varepsilon}(-\varphi_{vs} - b \cdot \Delta x)\right) & -\varepsilon - b \cdot \Delta x \leq \varphi_{vs} \leq \varepsilon - b \cdot \Delta x \\ 1 & \varphi_{vs} < -\varepsilon - b \cdot \Delta x \end{cases}$$

where $\varphi_{vs}$ is the void/solid distance function and $\Delta x$ is fixed and equal to $1\mu m$. Figure 3.3 shows the Heaviside function for three different b-factors. It can be seen from figure 3.3 that

the smeared Heaviside function has an opposite direction to the illustration shown in figure
3.2. This is because the void/solid signed distance function has to be negative in the void, as
shown in figure 3.4.
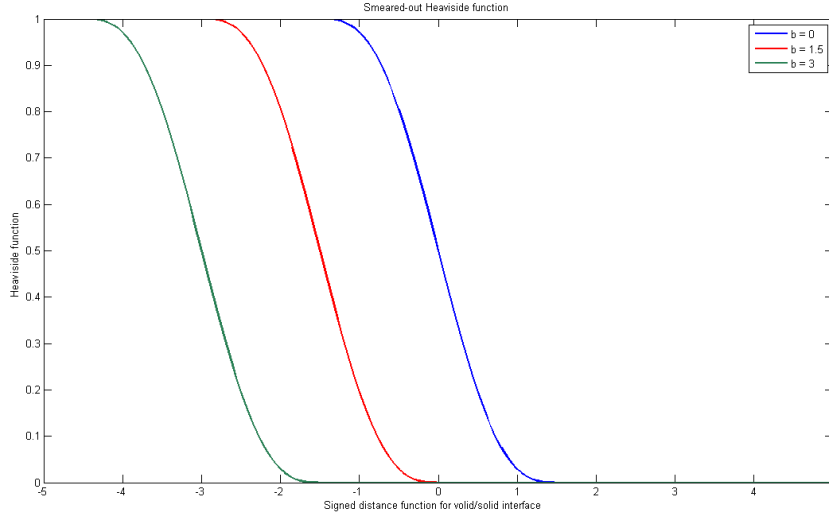


***Figure 3.3*** *The smeared Heaviside functions with b-factor equal to 0, 1.5 and 2.*

Furthermore the Dirac delta function will also shift as a consequence of the b-factor change.
The Dirac delta function has the following form,

$$\delta(\varphi_{vs}) = \begin{cases} 0 & \varphi_{vs} > \varepsilon - b \cdot dx \\ -\dfrac{1}{2\varepsilon} - \dfrac{\varphi_{vs}}{2\varepsilon} \cos\left(\dfrac{\pi}{\varepsilon}(-\varphi_{vs} - b \cdot dx)\right) & -\varepsilon - b \cdot dx \leq \varphi_{vs} \leq \varepsilon - b \cdot dx \\ 0 & \varphi_{vs} < -\varepsilon - b \cdot dx \end{cases}$$

Finally the interface is found when the signed distance function is equal to zero. This
corresponds to the interval $-\varepsilon \leq \varphi \leq \varepsilon$. To better understand this interval and the calculation
of the interface, figure 3.4 is shown. The figure shows an illustration of how the calculation of
the interfacial area shifts when the b-factor is changed, and the interval is implemented.
Figure 3.4a) is an illustration of the case when b=0, and figure 3.4b) shows the case when b is
larger than zero. Th green, red and blue line represents the signed distance functions area of
calculation. At the red line the signed distance function is equal to zero. The signed distance
function is also shown in the figure with the corresponding smeared Heaviside function.
Furthermore the space between the red line, to the blue and green is the same and is the
tolerance value. This tolerance value is as mentioned before the best value according to Osher
et al. [2003]. The ideal case for the simulation would be figure 3.4b). This is because as

shown in figure 3.4a) the outer most part of the function will intersect in the solid area. Decreasing the b-factor will give us a better approximation of interfacial area between the solid surface and the fluids. Furthermore figure 3.4 shows how the delta function is stationary as shown in figure 3.4b) while the Heaviside function is shifted. This concept is important to understand and in chapter 6 the optimal b-factor will be chosen in order to minimize the error of the interfacial area calculations.
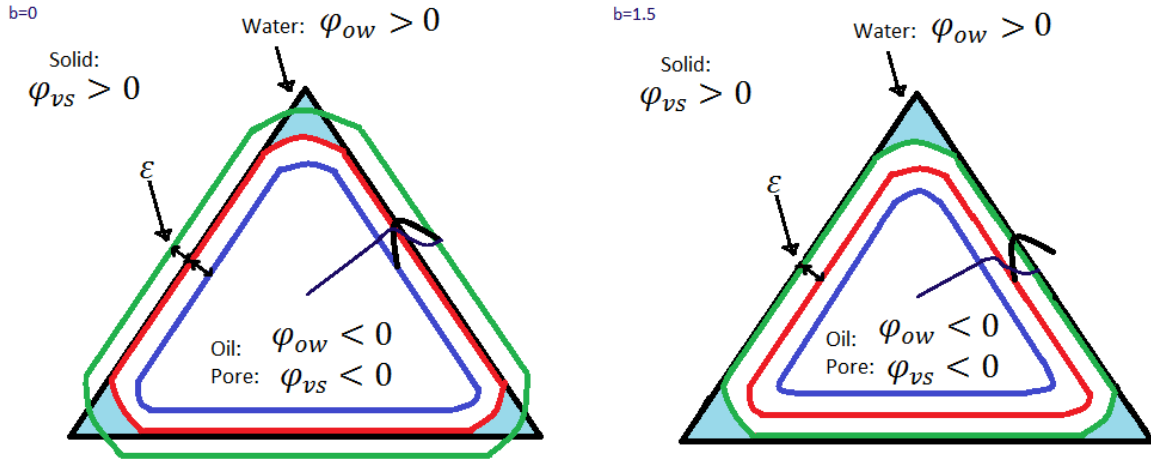


**Figure 3.4:** *Illustration of the Heaviside functions approach to interfacial area simulations for a) b=0 a) b larger than 0.*

Till now it has been explained to an extent how the model finds and excludes the thin film on the solid wall. To be able to compare the result from the simulation, an analytical approach has to be presented. The work done by Frette and Helland [2010] is used to analytically calculate the interfacial area of the curved section only. Figure 3.5 shows an illustration of the analytical approach for calculating the interfacial area between oil and water at the curvature only. For a simple geometry as a triangular the calculation is given in equation (3.34) Frette and Helland [2010].

$$A_{ow} = 2nr\beta = 2nr\left(\frac{\pi}{2} + \theta + \gamma\right)$$
(3.34)

where n is number of corners, $\beta$ is the angle between oil and water as shown in figure 3.5. As shown in the figure the pore corners will be occupied by the wetting phase (water) after an oil invasion. The interface in a corner can be represented by a circular arc meniscus with radius $r$ Frette and Helland [2010]. The radius is expressed by the Laplace formula for interfaces in two-dimensional pore spaces,

$$r = \frac{\sigma}{P_c} = \frac{1}{C} \tag{3.35}$$

where C is the interface curvature with units equal to $[\mu m^{-1}]$.Inserting this into equation yields the following analytical approach to calculating the interface area between oil and water:

$$A_{ow} = \frac{2n}{C}\left(\frac{\pi}{2} + \gamma\right) \tag{3.36}$$

The analytical approach is important to test the reliability of the level set model and is done so in chapter 6.
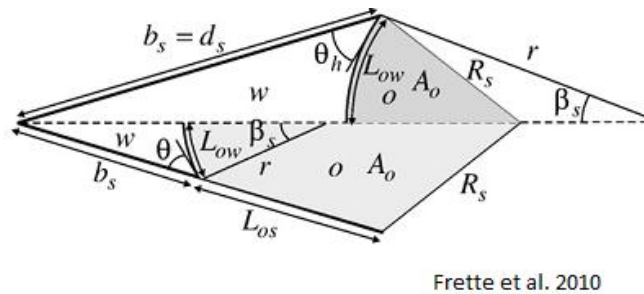
*Figure 3.5: Illustration of the analytical approach to calculating the interfacial area (Frette and Helland [2010].*

The following chapter gives a description of the input files the simulation model needs in order to give appropriate results.

# CHAPTER 4

# LEVEL SET MODEL FOR CAPILLARY-CONTROLLED DISPLACEMENTS

The first step in the level set code developed by IRIS is to read the input-files, which are images of the pore geometry and initial oil-water configuration. The subsequent step is to calculate the solid/void signed distance function and the oil-water signed distance function. After the signed distance function for both systems has been calculated, the simulation solves the level set equation. After each time step the process of reinitialization of the $\varphi_{ow}$ to the signed distance function takes place. The level set equation and its fluid-solid boundary conditions are solved and changed for each time step until steady-state is reached. Steady state is reached when the convergence criteria is fulfilled. The convergence criterion is given in equation (4.1) below.

$$\frac{\sum_{i,j,k}\left|\varphi_{ijk}^{n+1} - \varphi_{ijk}^{n}\right|}{N} < tol \cdot \Delta x \tag{4.1}$$

Equation (4.1) sums up all the errors for each grid point divided by the total number of points. That number has to be smaller than the tolerance ($tol$) multiplied by $\Delta x$. The tolerance in our simulation is set equal to 0.002 and $\Delta x$ is equal to $1\mu m$, which is the voxel size. The convergence criterion is determined by comparing $\varphi_{ow}$ after each reinitialization. Furthermore the input and output files are described below.

**Input and output files**

The following input files are read by the level set code:

**image.dat**: An image of the geometry of the porous medium.

**init_ow_conf.dat**: The initial oil- and water configuration.

The following files are simulated by the program:

**geometry.dat**: Gives a black and white image of the porous medium. Solid = 1, void = 0.

**initial_fluid_config.dat**: Gives a black and white image of the initial fluid configuration, water = 1, oil = 0.

**phi.dat**: The void-solid signed distance function, phi < 0 in void and phi > 0 in solid.

**phi_ow_error_xxxx.dat**: Data-file with total error after each iteration step for the given capillary pressure step 'xxxx'. Column 1: iteration, Column 2: error.

**Pc_Sw_aow_xxxx.dat**: Data-file with capillary pressure, volume and areas at capillary pressure step 'xxxx' calculated in the entire computational domain. Column 1: input interfacial curvature (=capillary pressure/interfacial tension), Column 2: Volume of oil, Column 3: Volume of pore space, Column 4: Volume of solid phase, Column 5: Surface area between void and solid, Column 6: Area between oil and water neglecting the contribution from thin water films coating the solid surface.

**Pc_Sw_aow_subset_xxxx.dat**: Data-file with capillary pressure, volume and areas at capillary pressure step 'xxxx' calculated in a specified subset of the computational domain. Column 1: input interfacial curvature (=capillary pressure/interfacial tension), Column 2: Volume of oil, Column 3: Volume of pore space, Column 4: Volume of solid phase, Column 5: Surface area between void and solid, Column 6: Area between oil and water neglecting the contribution from thin water films coating the solid surface, Column 7: Area between oil and water including the contribution from thin water films coating the solid surface.

**phi_ow_xxxx.dat**: Oil-water level set function for stable fluid configuration at the specified capillary pressure step 'xxxx', where phi_ow < 0 in oil, phi_ow > 0 in water. A Matlab-file "plot_data.m" plots the fluid configuration based on the phi_ow-data.

## 4.1 Boundary conditions

In the simulation the boundary conditions are changed in such a way that the oil phase enters the porous medium from only one side in the cube. In the integer array $inlet[a, b, c, d, e, f]$ the user is able to input at which side of the cube the oil will enter. The array gives all faces of the void/solid image that are specified by 1 as the inlet boundary while all other boundaries specified by 0. The drainage simulation is done for all sides of the cube. The imbibition simulation is done for a number of interface curvatures, but only for the sides where $z = 0$ and $z = L$.

Furthermore the integer array $periodic[a, b, c, d, e, f]$ specifies the boundary conditions at all the faces of the void/solid image. The faces that are specified to be inlet boundaries in $inlet[a, b, c, d, e, f]$ must have value -1 in $periodic[a, b, c, d, e, f]$, because linear

extrapolation is assumed at inlet boundaries. At all other boundaries, mirror-reflected conditions are used, and this corresponds to the value 2 in the array $periodic[a, b, c, d, e, f]$. The parameter $outlet[a, b, c, d, e, f]$ is not used and all its elements are set to 0.

At the inlet boundaries a layer with thickness *inlet_layer_thickness* with pore space filled with invading fluid is added to the computational domain, and n[] is updated accordingly. The parameter *n_crop* represents the updated first and last index in the x-, y- and z-directions of the subdomain without the layer added.

Figure 4.1 shows an example in two dimensions for how the pore space filling simulation undergoes. The figure shows an inlet boundary $at\ x = n[0] - 1$ and $y = 0$. The boundary conditions of the computational domain are mirror reflected, periodic and linear extrapolated at the inlet boundary. And as shown in figure 4.1 at the inlet boundary, 2-3 layers of invading fluid will be added.
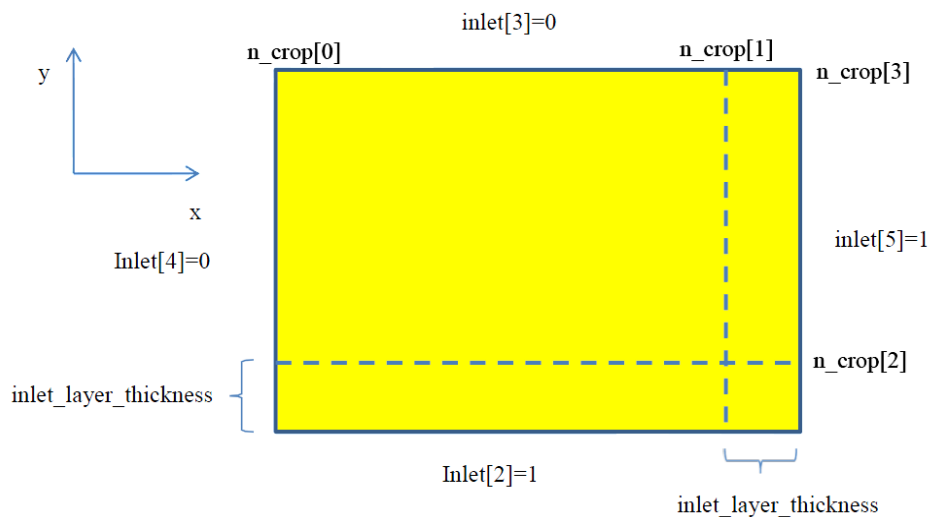


***Figure 4.1****: Two dimensional example of the filling at the inlet boundary.*

# CHAPTER 5

# CAPILLARY PRESSURE, WATER SATURATION AND INTERFACIAL AREA RELATIONSHIP

The interfacial area between many fluid-fluid configuration play a critical role in many subsurface multiphase flows and transport processes (Porter et al. 2010). In the past decade there have been a lot of investigations to grasp the relationship between the capillary pressure, water saturation and interfacial area. There are well known examples of the $P_c - S_w$ relationship, but not much for the $P_c - S_w - a_{ow}$ relationship. Porter et al. [2010] mention that there are two contributions to the total interfacial area between two immiscible fluids. The two contributions are the capillary pressure induced area, and thin film-associated interfacial area. Capillary associated interfacial area consists of all nonwetting interfaces in contact with the bulk, mobile wetting-phase and wetting-phase pendular rings (Porter et al. 2010). Furthermore according to the article by Porter et al. 2010 the film associated interfacial consists of the nonwetting phase in contact with the wetting phase films that exist on solids of pores occupied by the nonwetting phase. Figure 5.1 shows the fluid contact contributions that lead to the total fluid-fluid interfacial area.
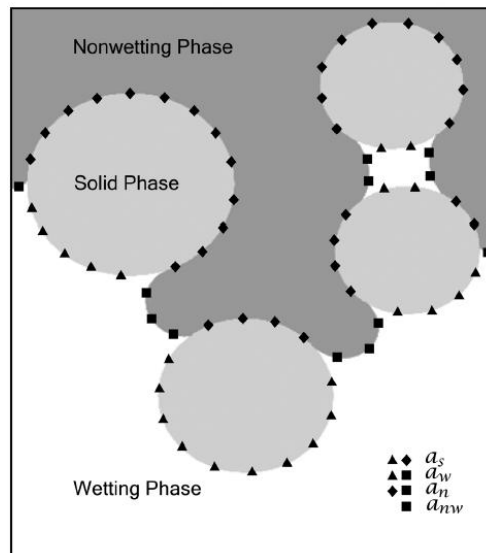


*Figure 5.1: Illustration of the fluid-fluid contact contributions and interfacial area (Porter et al. 2010).*

The figure shows an illustration of the interfacial area contributions for every phase in an oil and water system. The interfacial area which is of interest for our study is the interfacial area between oil and water. The interfacial area between oil and water is denoted as $A_{ow}$. The interfacial area as calculated in the level set method is shown in equation (5.1.)

$$A_{ow} = \int_{\Omega} \delta(\varphi)|\nabla\varphi|d\vec{x}$$

(5.1)

In the simulation results the interfacial area will be denoted as the specific interfacial area, which is the equation given above for interfacial area divided by the total volume of the pore media. Equation (5.2) gives the specific interfacial area as a function of bulk volume and total interfacial area.

$$a_{ow} = \frac{1}{V}\int_{\Omega} A_{ow}\,dx$$

(5.2)

where V is the total volume of the porous system under study.

In work done by Hassanizadeh and Gray [1993] they proposed that an inclusion of the interfacial area variable in the $P_c - S_w$ relationship could aid to eliminate the hysteresis that is commonly observed in the $P_c - S_w$ relationship. Furthermore results from the work done by Joekar-Niasar et al. [2007] concluded that the interfacial area can be an essential variable in the capillary pressure and saturation relationship for multiphase flow. However not much experimental investigations concerning the relationship between $P_c, S_w$ and $a_{ow}$ has been done. Only a few measurements have been reported in the literature (Porter et al. 2010), such as Culligan et al. [2004, 2006] amongst a few others. However none of them looked at the direct relationship between $P_c$, $S_w$ and $a_{ow}$. The literature review by Porter et al. [2010] concludes that there has not been much experimental study which the writer is aware of that focuses on characterizing the $P_c - S_w - a_{ow}$ relationship. However a number of pore scale modeling techniques have been used to investigate the direct $P_c - S_w - a_{ow}$ relationship. A number of pore network models have been developed and they all give a variety of characteristics for the $P_c - S_w - a_{ow}$ relationship (Porter et al. 2010). For example the work done by Helland and Skjæveland [2007] showed that the shape of the surface was sensitive to contact angle hysteresis, while the work done by Joekar-Niasar et al. [2009] and Held and Celia [2001] showed that there a slit anticline shape of the interfacial area when plotted against water saturation. There have also been a few Lattice-Boltzmann simulations of the

$P_c - S_w - a_{ow}$ relationship, like the one by Porter et al. [2009], which also showed that the modeled interfacial area exhibited the anticline curvature along the $S_w$-axis. Porter et al. [2010] measured the capillary pressure, water saturation and interfacial area of the wetting and nonwetting phase for drainage and imbibition for a cube pack. This is of relevance to our study, because we are also looking at a sphere cube pack in the our simulations. Figure 5.2 shows the experimental result from their work for interfacial area as a function of water saturation for both the total IFA and capillary associated IFA.
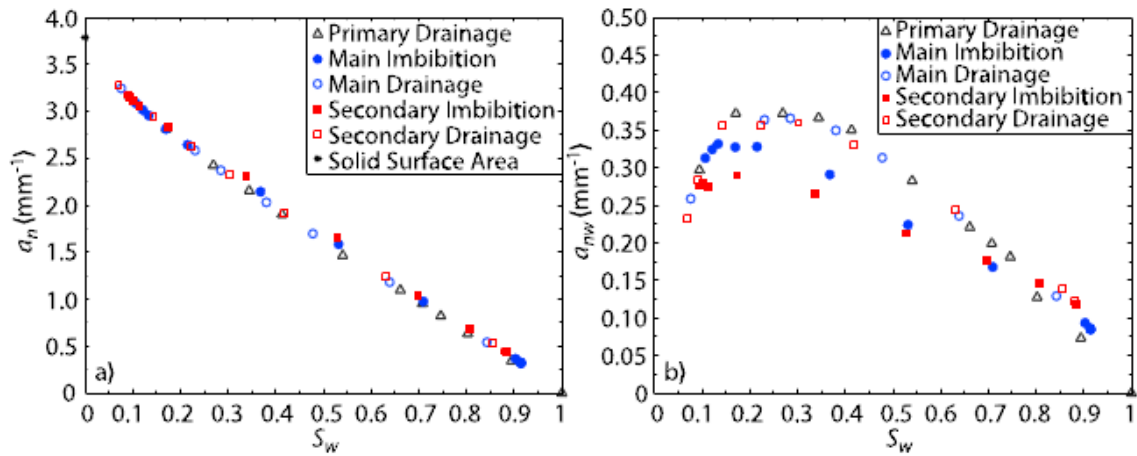


*Figure 5.2:* *Result of experimental data for the interfacial area as a function of water saturation for a) total IFA, $a_n$ b) capillary associated IFA, $a_{nw}$ (Porter et al. 2010).*

Figure 5.2 a) shows that there is no hysteresis observed when looking at the total IFA, however there is hysteresis in the capillary associated IFA. Furthermore Porter et al. [2010] also plotted a three dimensional plot of the $P_c - S_w - a_{ow}$ relationship. The result is shown in figure 5.3.
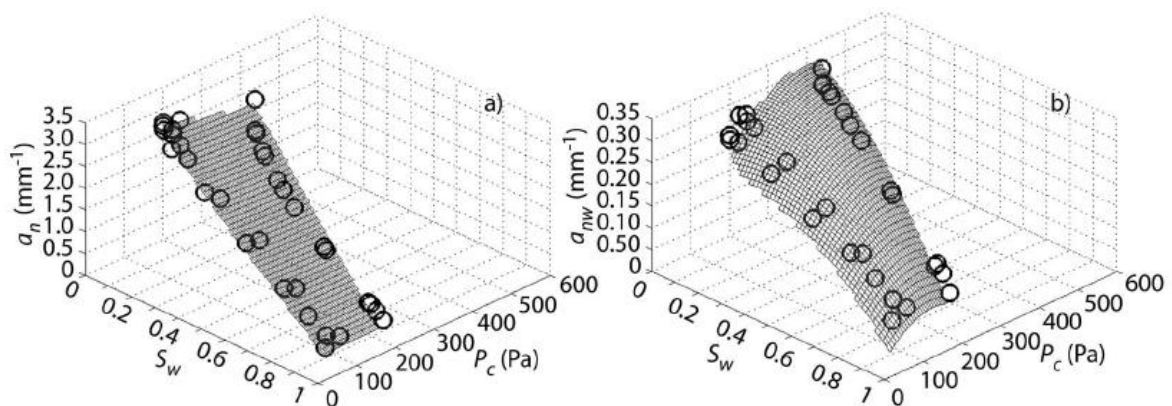


*Figure 5.3:* *Best fit surface plot for the experimental a) $P_c - S_w - a_n$ data b) $P_c - S_w - a_{nw}$ data (Porter et al. 2010).*

The surface plot shown in figure 5.3a) looks very flat, and is due to the linear result shown in figure 5.2a). However for the capillary associated IFA, the relationship has a slight convex curve. Both figures indicate that the capillary associated IFA exhibit hysteresis. We may ask ourselves what is needed to eliminate hysteresis from the $P_c - S_w$ relationship. Will inclusion of the interfacial area reduce this difference? Chapter 6 presents the result from all simulations done in our study. The results are used to compare with experimental results from previous work to validate the reliability of the model, and also to try to answer the question stated above.

# CHAPTER 6

# SIMULATION RESULTS AND DISCUSSIONS

In the following chapter simulation results and interpretations are presented. The output files that where explained in chapter 4 are read in Matlab, and the results are used to graph curves in Excel. Three dimensional plot of the data where done in Matlab, and the visualization of the interface between oil and water for predefined interface curvature is done in Paraview. The calculations and results are based on a synthetic cube pack. The size of the synthetic cube pack is $50 \times 50 \times 50$ voxels. The voxel size is set equal to $\Delta x = 1\mu m$ as mentioned before. The length of the cubic sphere pack is therefore equal to $L = 50 \cdot \Delta x = 50\mu m$. Figure 6.1 shows the cube simulation for the void solid space and its corresponding coordinate system. For the drainage process if $z = 0$ then the inlet is on the top surface and the nonwetting phase fluid invades on the same side, hence it moves in negative z-direction, and if $z = L$ the inlet of the nonwetting fluid is on the bottom surface and the invading fluid i.e. oil moves in positive z-direction. The imbibition process can be explained in the same manner, but the water will be the invading fluid. All figures in simulated in Paraview are of the oil displacement drainage process will be represented by the color red and the imbibition process by the color green.
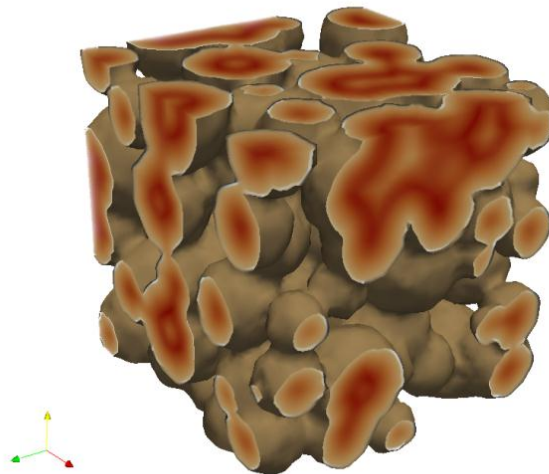


*Figure 6.1:* *Void/solid cube and its corresponding coordinate system visualized in Paraview.*

Also important to note is that most of the result presented is of the subset pack, which is a cube within the sphere pack. If that is not the case it will be noted as the "total" sphere pack. To test the reliability of the model a simulation for a triangular shaped pore is done in Matlab. The result is shown in figure 6.2. The figure shows how the oil/water interface move as the capillary pressure increases. The green line represents the interface between the solid and void, the pink, blue and yellow line show the evolution of the oil/water interface. The figure confirms theory that as the capillary pressure increases, the nonwetting fluid will occupy a larger area than the wetting phase.
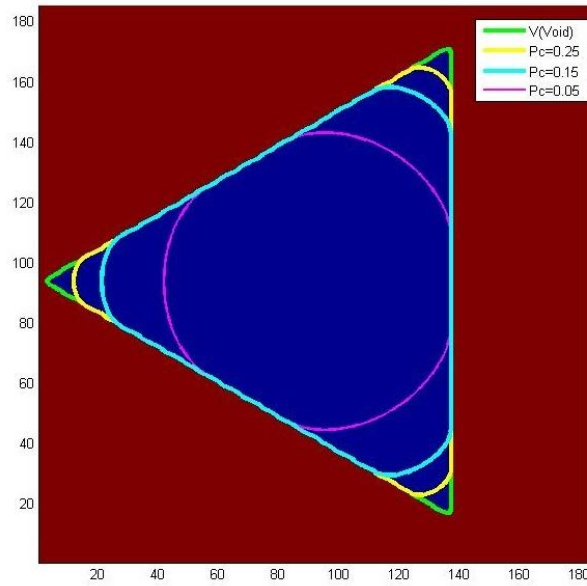


*Figure 6.2: Result from Matlab simulation for increased capillary pressure.*

The interfacial area that can be represented as the thin film on the solid wall can be excluded by using equation (3.34) as mentioned before. In our example the number of corners is set equal to 3. The contact angle between oil and water is set equal to 0 and the surface tension equal to 1. Example of analytical calculation of the interfacial area for C=0.25:

$$A_{ow} = \frac{2 \cdot 3}{0.25[\mu m^{-1}]}\left(\frac{\pi}{2} + \frac{30° \cdot \pi}{180°}\right) = 0.018689 \ [\mu m^2] \tag{6.1}$$

Furthermore the analytical approach is compared to the model to determine the best value for for the b-factor. Figure 6.3 show the result for the interfacial area between oil and water for a number of different b-factors as a function of interface curvature. As can be seen from the figure the low b-factor is nowhere near the analytical results compared to higher b-factors. Figure 6.4 show the result of the b-factor for values of 1.5 and higher.
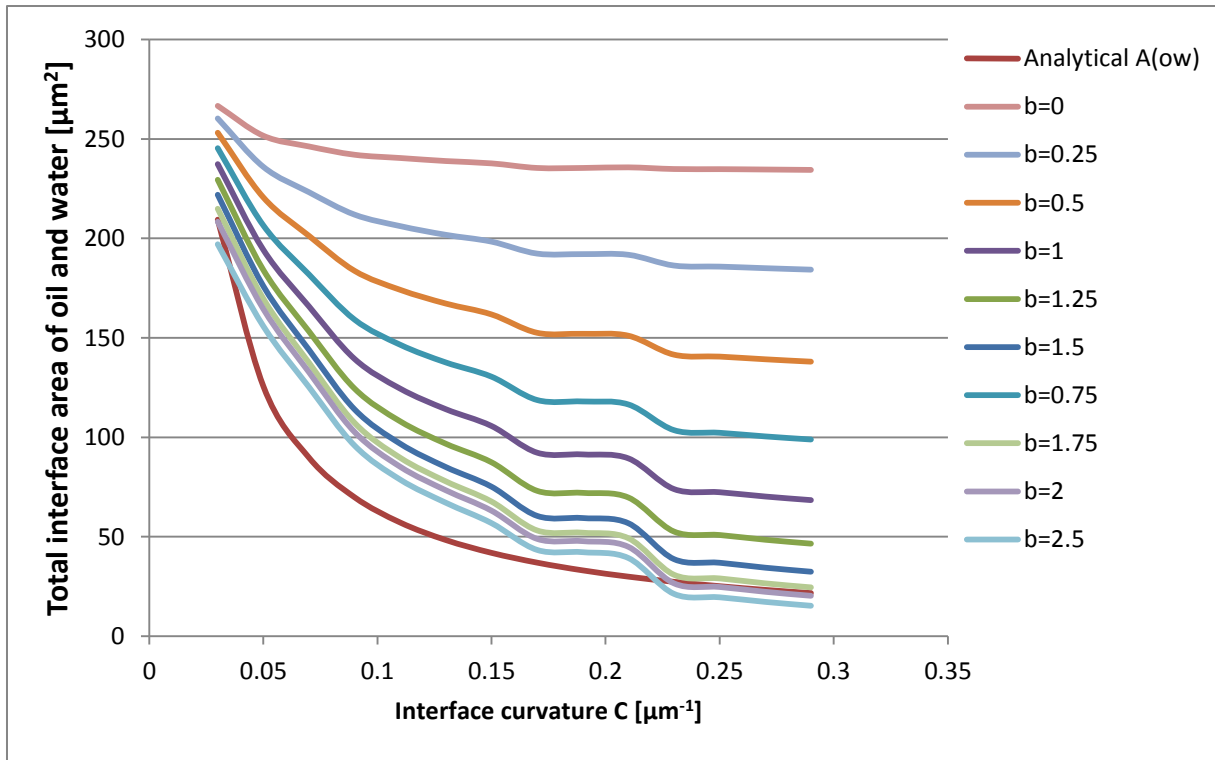
*Figure 6.3:* *Interface area of oil and water as a function of interface curvature.*
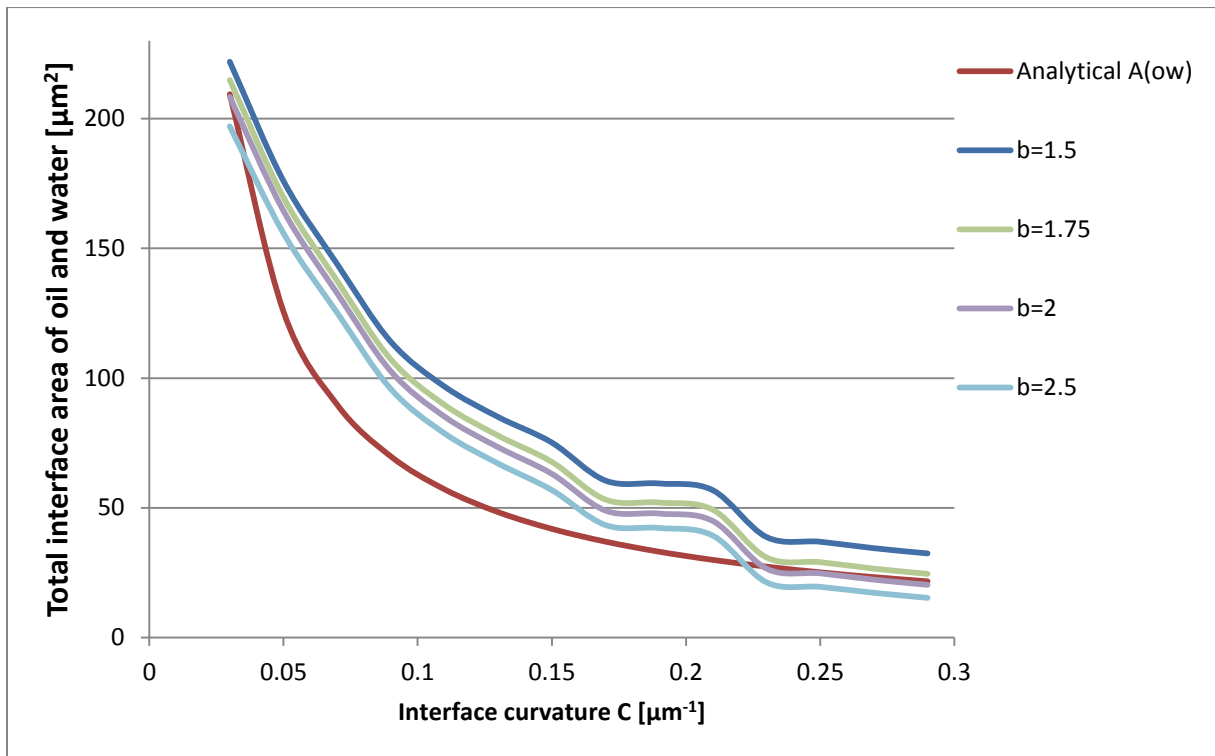


*Figure 6.4:* *Interface area of oil and water as a function of interface curvature for values b=1.5 and higher.*

Figure 6.4 shows us that a b-factor between $b = 1.5$ and $b = 2$ seems to correspond the best according to the analytical result. Therefore it may conclude that $b = 2$ is the best choice, but this is not the case. Recall figure 3.4 which showed an illustration of how the model simulates the results depending on the value of the b –factor. If we choose a value lower than $b = 1.5$, the model will include oil-water interfacial area contributions from interfaces that coincide with the solid phase. This can be explained by figure 3.4 and equation (3.28) for the interfacial area which is given in chapter 3.5. Equation (3.28) gives the interfacial area between oil and water as the integral of Dirac delta function multiplied by the Heaviside function. To be able to fully grasp the concept and which value of b gives the best result, the delta function and the Heaviside function used in the simulation is plotted in Matlab. The results are shown in figure 6.5 and for the b-factor 0, 1.5 and 2 only. Appendix A.3 has the full Matlab code for the reader if it is desired to test for other b-factors. Recall that the interfacial area is calculated by multiplying the Heaviside function with the Dirac delta function. Furthermore if we consider the interval mentioned in chapter 3, $-\varepsilon \le \varphi \le \varepsilon$, which is the interval that should represent the interface and plus a tolerance value more of the signed distance function. If we look at the first figure, where b=0, the interfacial area at the solid phase will be concluded in the calculations. Because as mentioned before, if the signed distance function is positive it will be on the solid phase, however if it is negative it will be in the void phase. Furthermore both figures for b=1.5 and b=2 are equal to zero at this section, which means that there is no calculation of the interfacial area in the solid phase. However as seen in the last figure, where b=2 the shift is too far to the left. If we consider figure 3.4 in chapter 3 and imagine the green line being shifted more inward. Then the model will not account for any interfacial area at solid phase, which can be a positive thing. However this will cause a loss in the interfacial area at the corners of the triangular pore. The best result would be to have a b-factor as the one shown in the right side of figure 3.4, one that barely touches the solid phase. A b-factor corresponding to that will give a better accordance with the analytical result because it will also include the interfacial area if the surface is rugged. Figure 6.6 shows the interfacial area of the different b-factors as a function of water saturation. The figure indicates that for lower water saturations the interfacial area has a much larger difference for the various b-factors. This can be explained by the fact that at lower water saturation the corners in the pore will be filled with oil, and a small b-factor will result in a higher uncertainty for the interfacial area. An analytical calculation of the interfacial area as a function of water saturation would be of essence to be able to compare the results. However this calculation was not conducted, but it can be concluded from the result
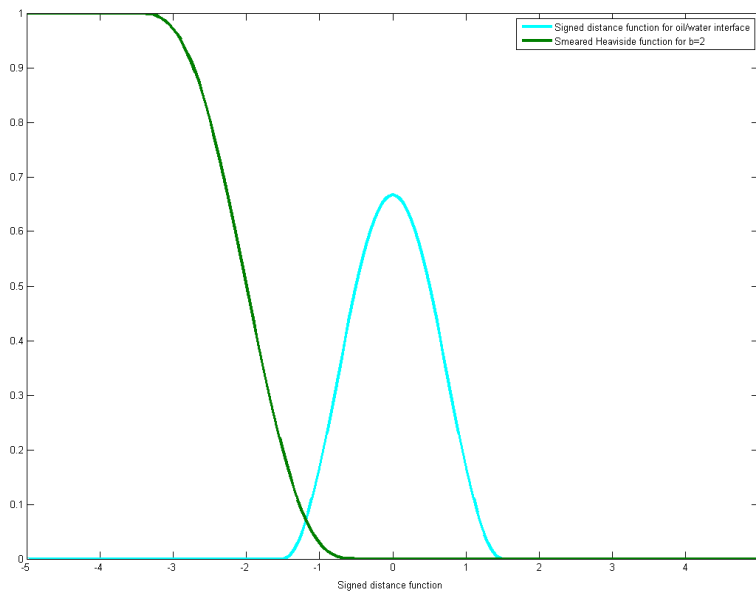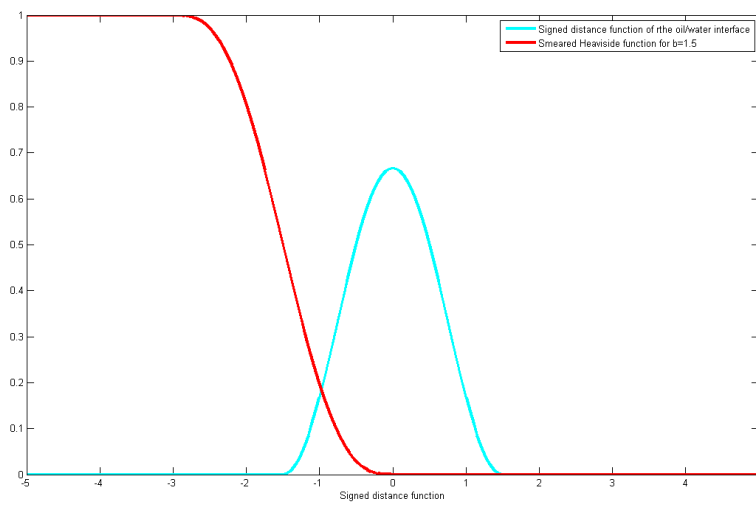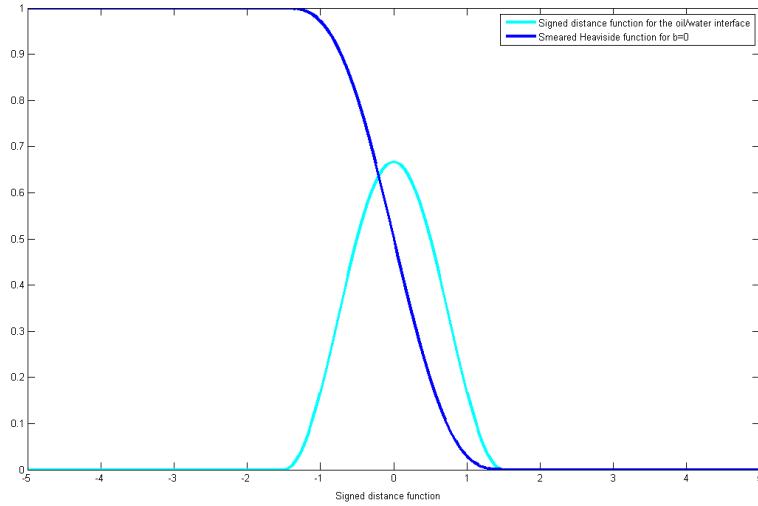
*Figure 6.5:* *The dirac delta function and the Heaviside function for b-factor equal to 0, 1.5 and 2.*
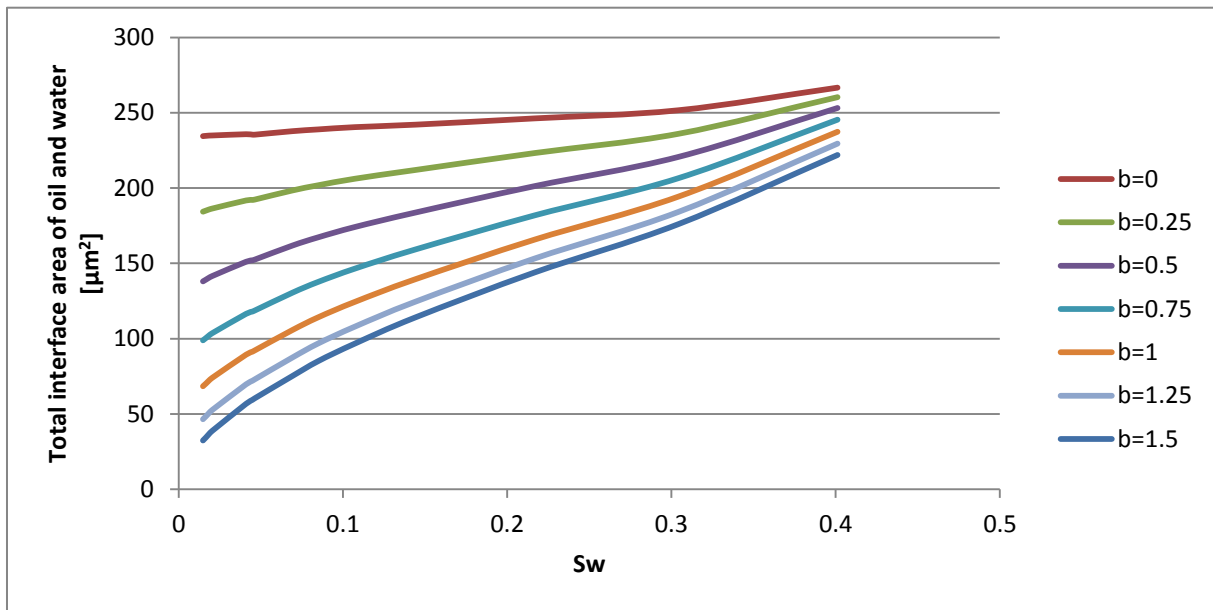
***Figure 6.6:*** *Interface area of oil and water as a function of water saturation for the different b-factors.*
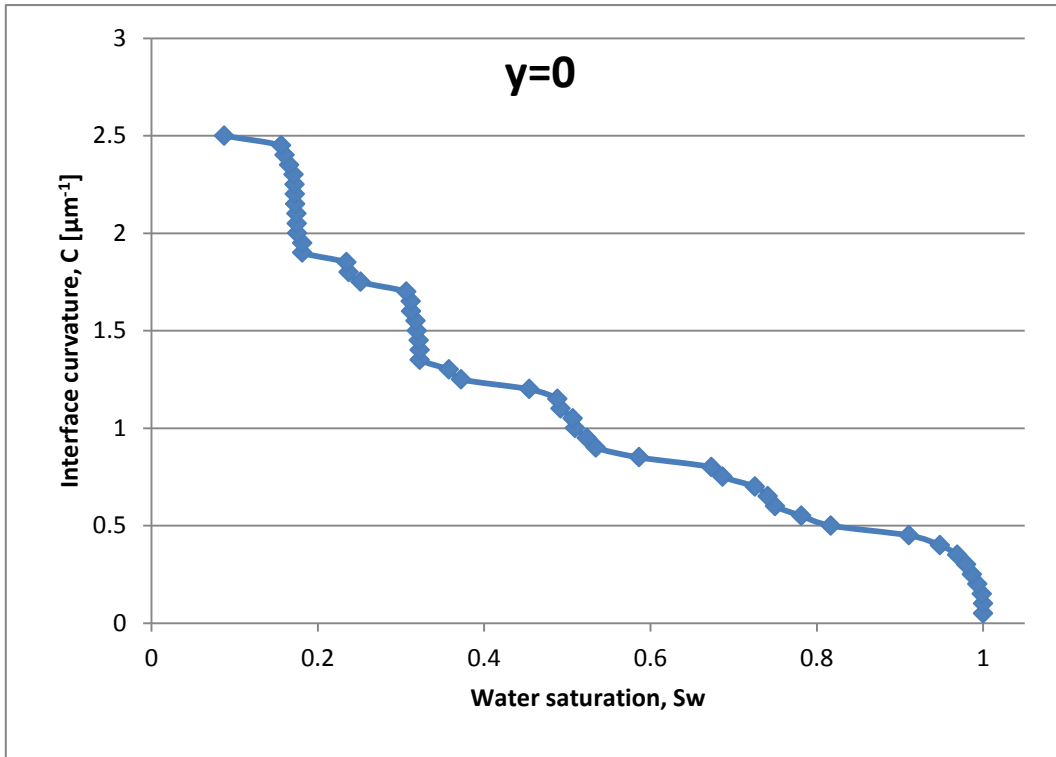
shown in the previous figures that the best choice for the b-factor is b=1.5, which is the number implemented in the simulation. The drainage results for invasion at different sides of the sphere pack are given in figures 6.7 to 6.12.
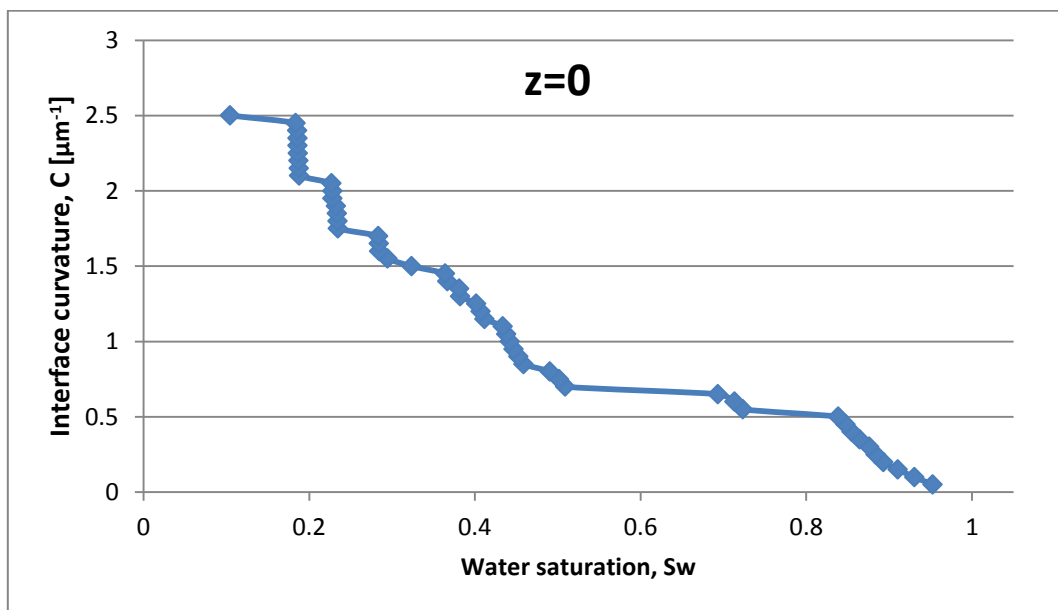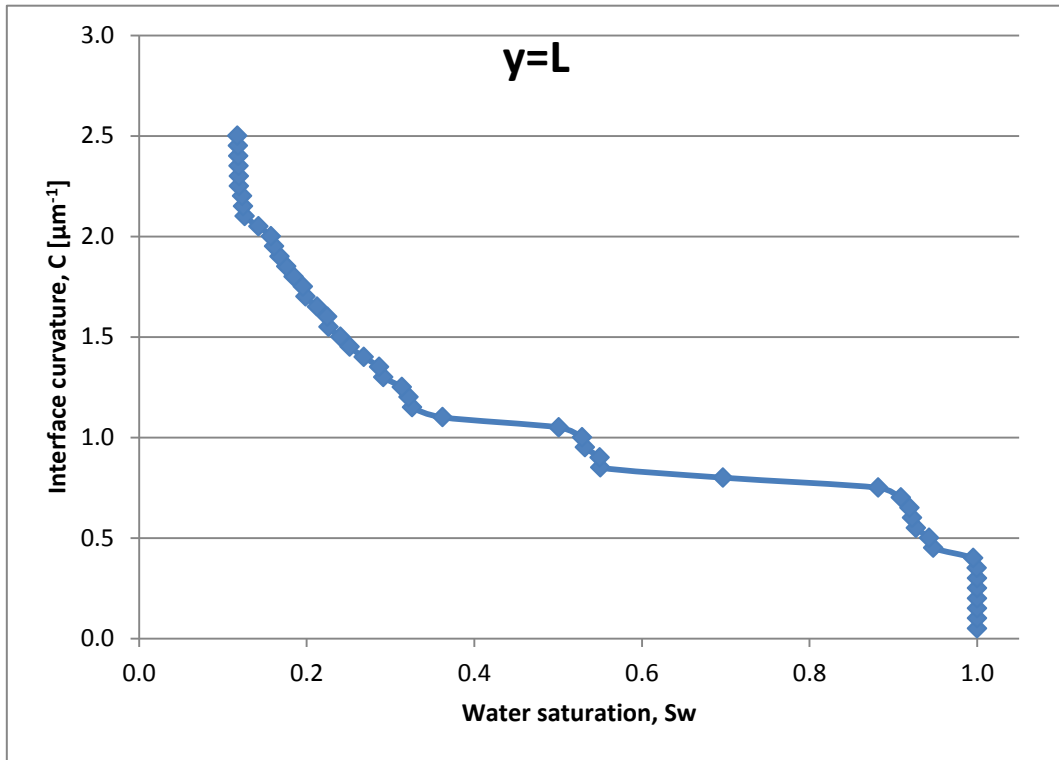


***Figure 6.7:*** *The drainage curve for invasion at z=0.*
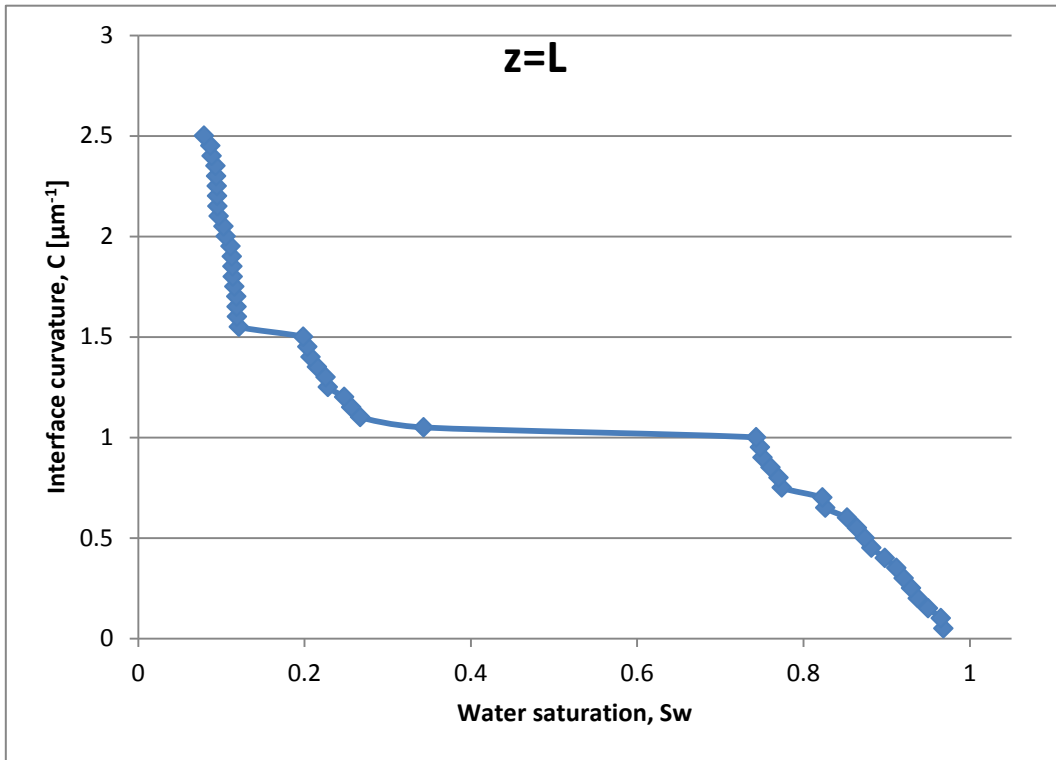
***Figure 6.8:*** *The drainage curve for invasion at z=L.*



***Figure 6.9:*** *The drainage curve for invasion at y=0.*

***Figure 6.10:*** *The drainage curve for invasion at y=L.*
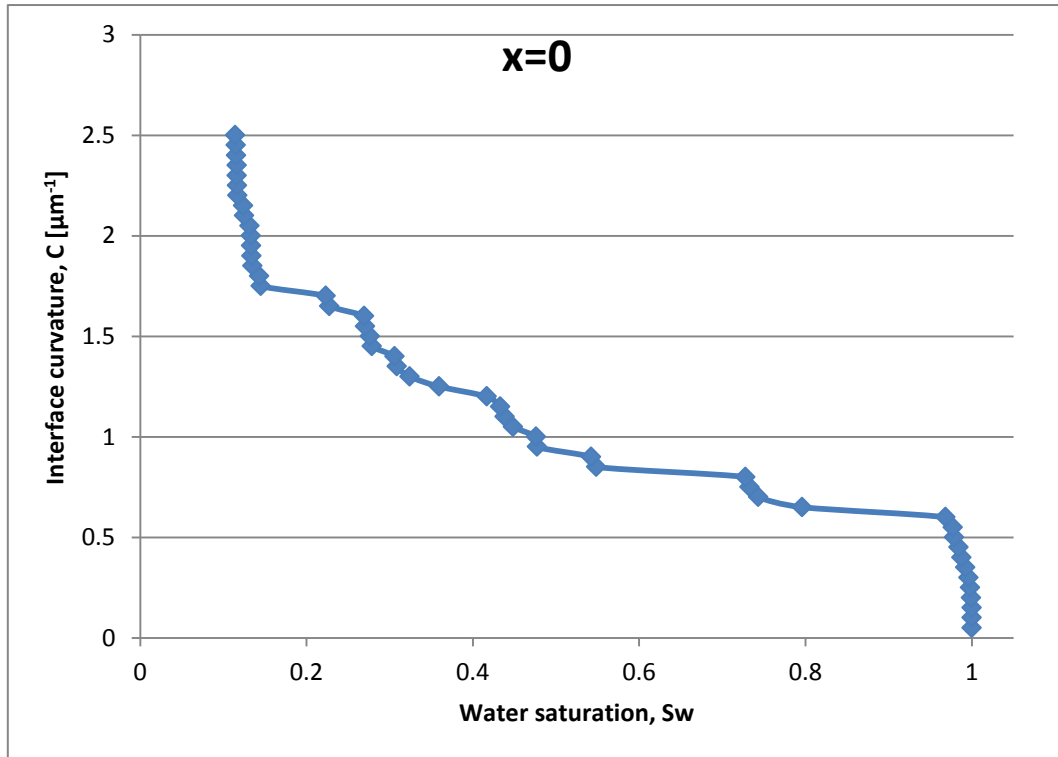


***Figure 6.11:*** *The drainage curve for invasion at x=0.*
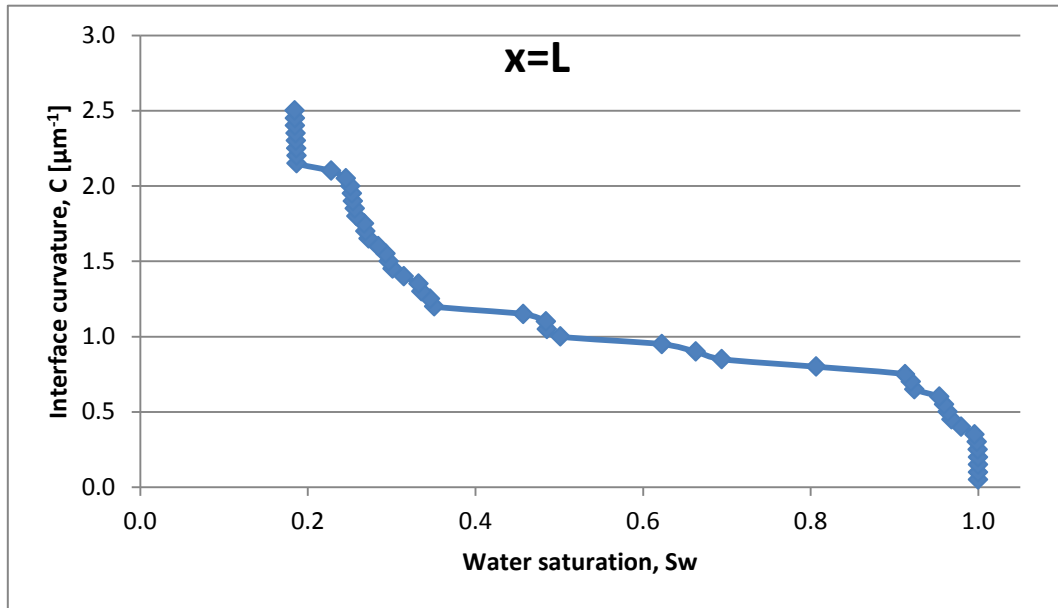
*Figure 6.12:* The drainage curve for invasion at x=L.

The drainage curves are simulated well, and show that the capillary pressure curves will be different for invasion in different sides of the sphere pack. Figure 6.13 shows all the drainage curves in one figure, the largest difference is for curve z=L and x=L.
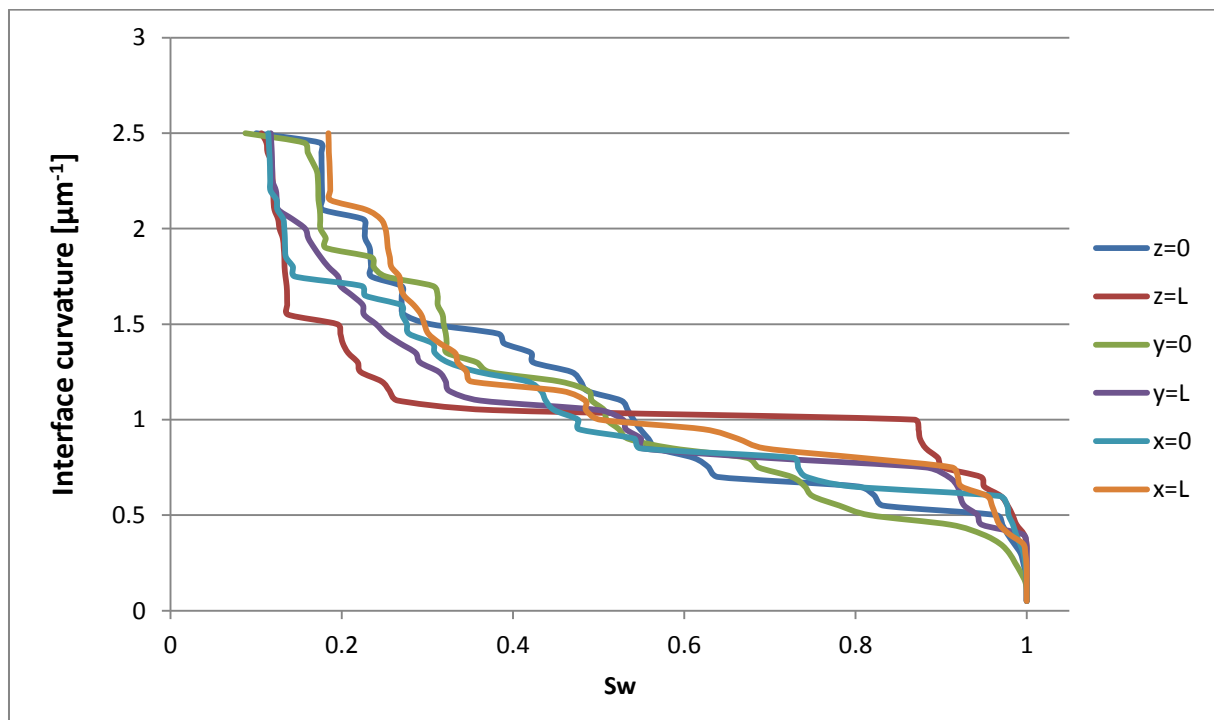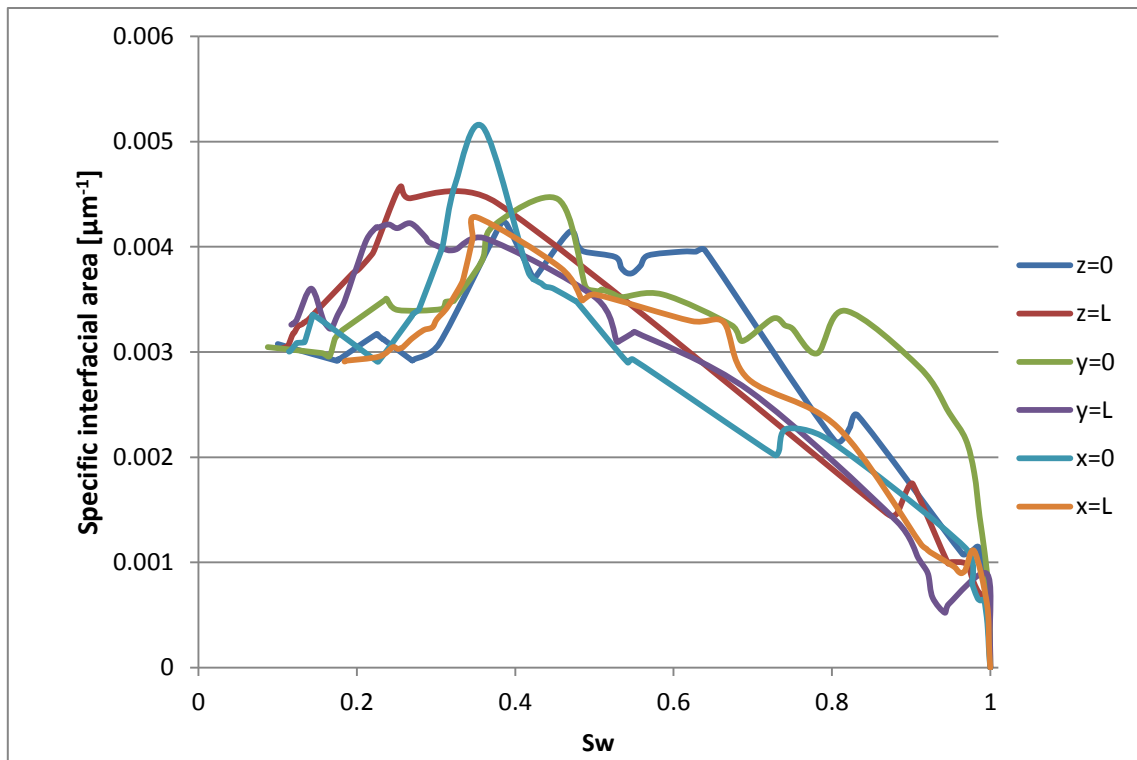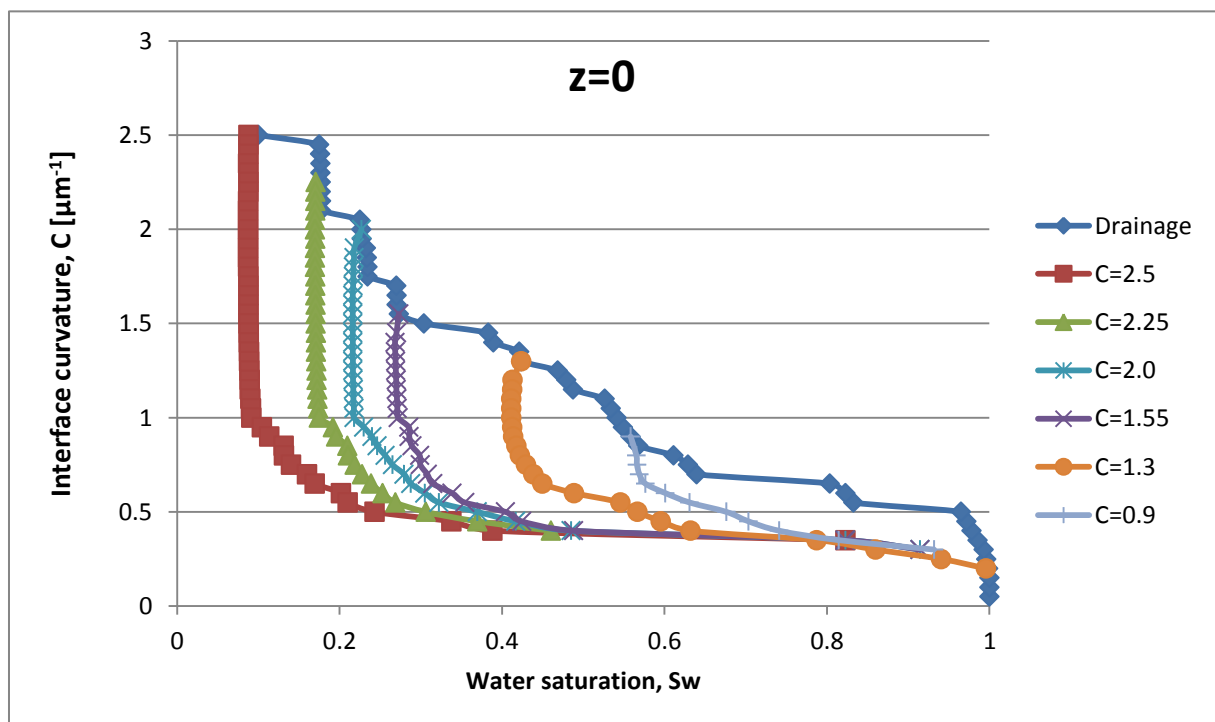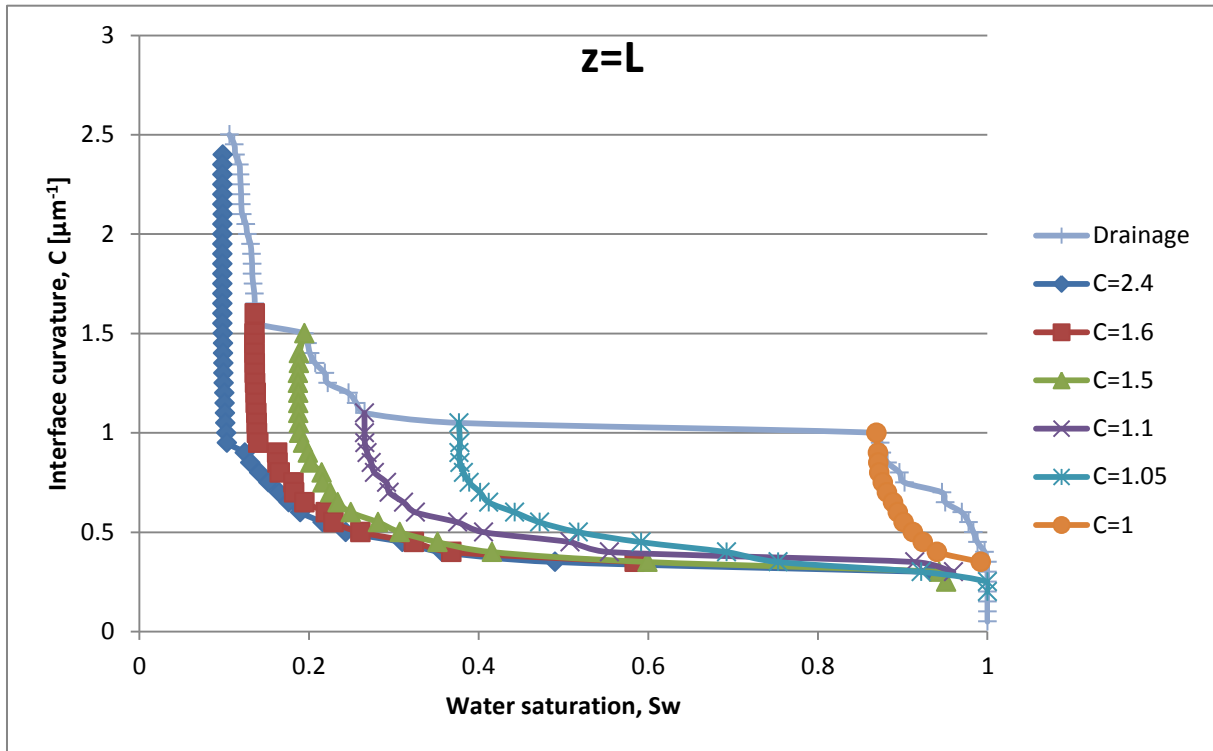


*Figure 6.13:* The specific interfacial area between oil and water for the subset pack.

Figure 6.13 also shows a large saturation jump at z=L compared to the other figures, this can also be seen in figure 6.7. Because the process is drainage this abrupt change in water saturation is an example of a Haines jump.
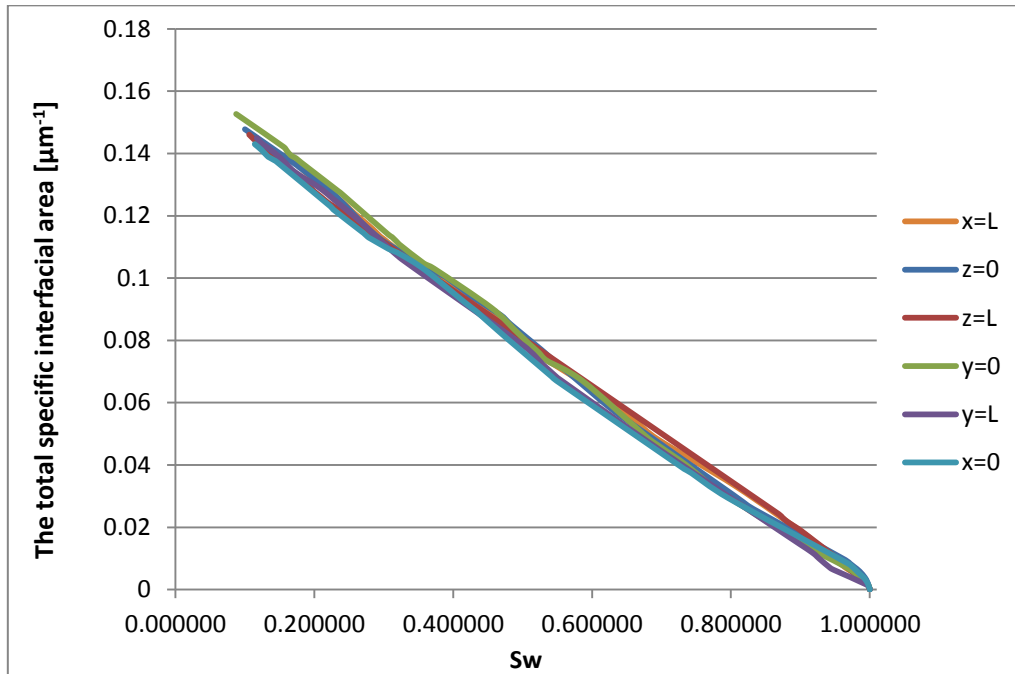


***Figure 6.14:*** *The total specific interfacial area between oil and water as a function of water saturation.*

Figure 6.14 shows the total specific interfacial area between oil and water as a function of the water saturation. The result is linear and compared to the result by Porter et al. [2010] it coincides well. Figure 6.15 shows the result in the subset pack, and has the characteristic convex shape that can also be seen in the result by Porter et al. [2010]. Figure 6.16 and 6.17 show the drainage curve and their corresponding imbibition curves for invasion at z=0 and z=L, respectively. The figures seem to correspond well with theoretical results (See figure 1.2). Figure 6.18 and 6.19 give $a_{ow}$ as a function of $S_w$ for the imbibition process at invasion for z=0 and z=L, respectively. Again the figures have the convex shape as mentioned before. Figure 6.20 compares $a_{ow}$ from drainage and imbibition for invasion at z=0 and z=L. The figure shows that the specific interfacial area is much higher for the imbibition compared to drainage. Figure 6.20b) shows that for low water saturation the specific interfacial area is almost identical for drainage and imbibition. The reason for higher interfacial area between oil and water could be due to the hysteresis events that are simulated by the model.

**Figure 6.15:** *The specific interfacial area between oil and water for the subset pack.*



**Figure 6.16:** *The specific interfacial area between oil and water for the subset pack.*

**Figure 6.17:** *The specific interfacial area between oil and water for the subset pack.*
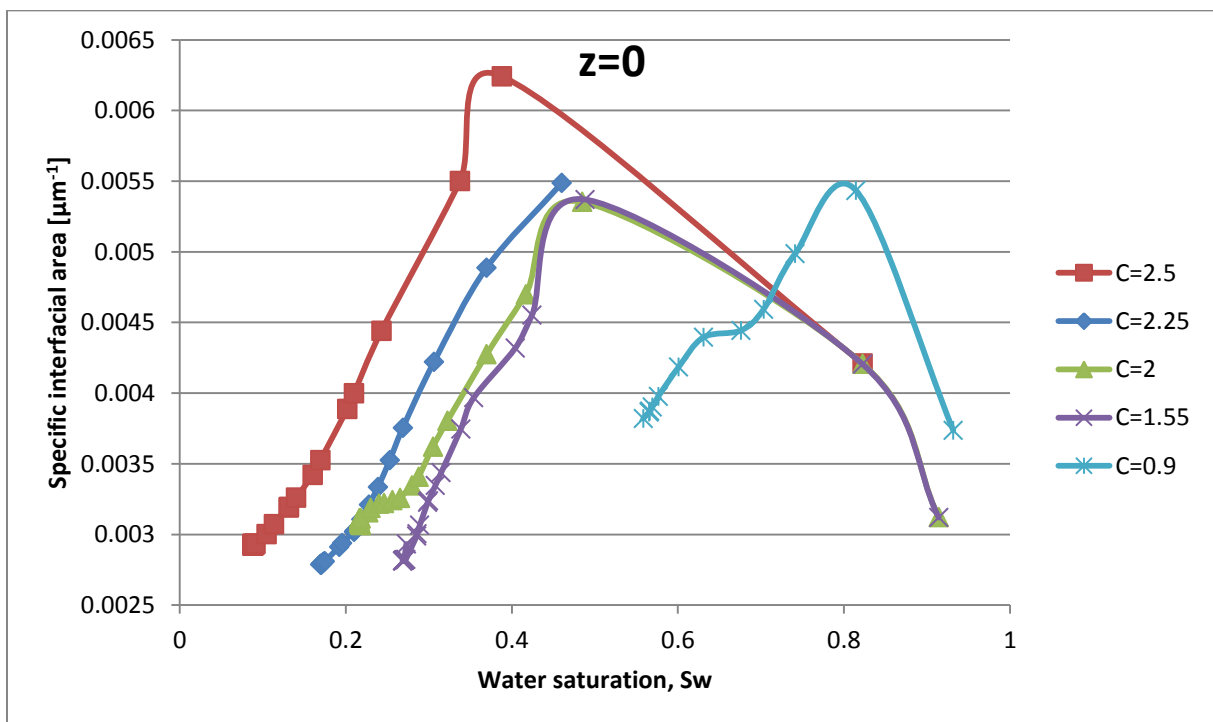


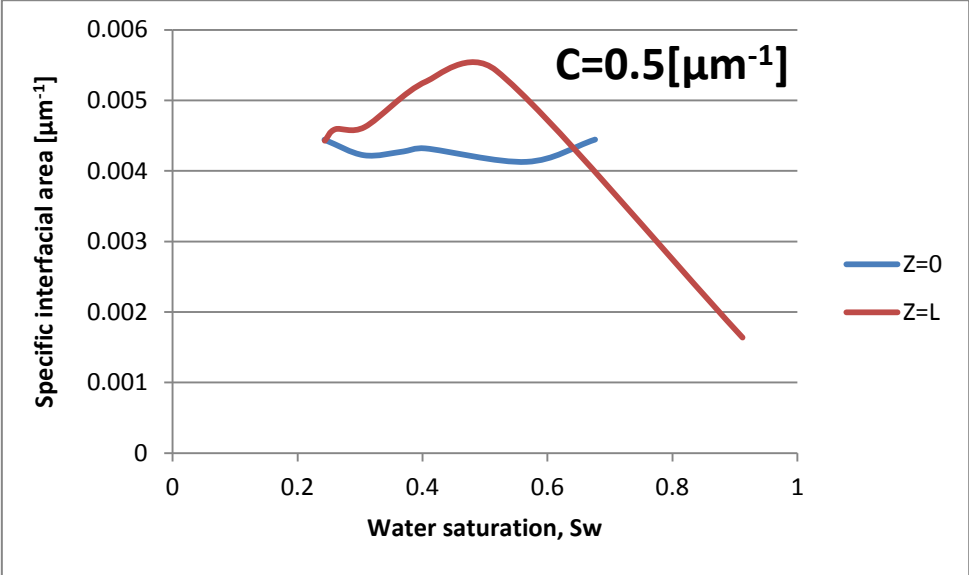**Figure 6.18:** *The specific interfacial area between oil and water for invasion at z=0.*
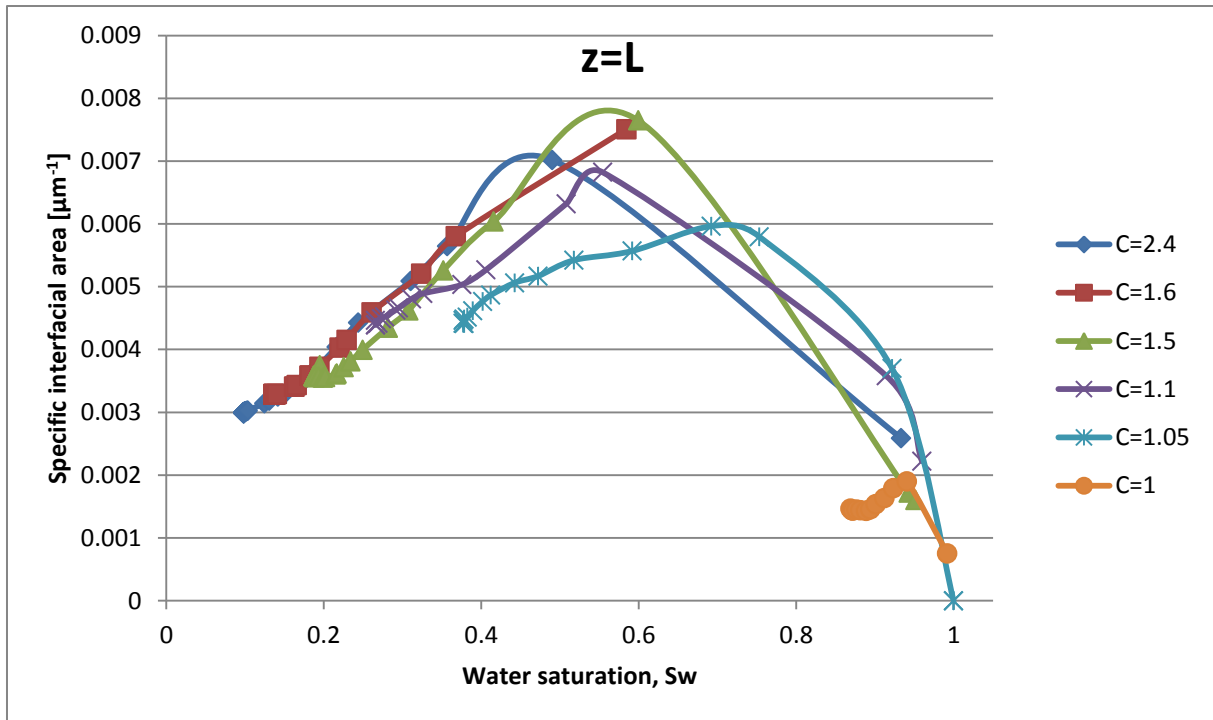
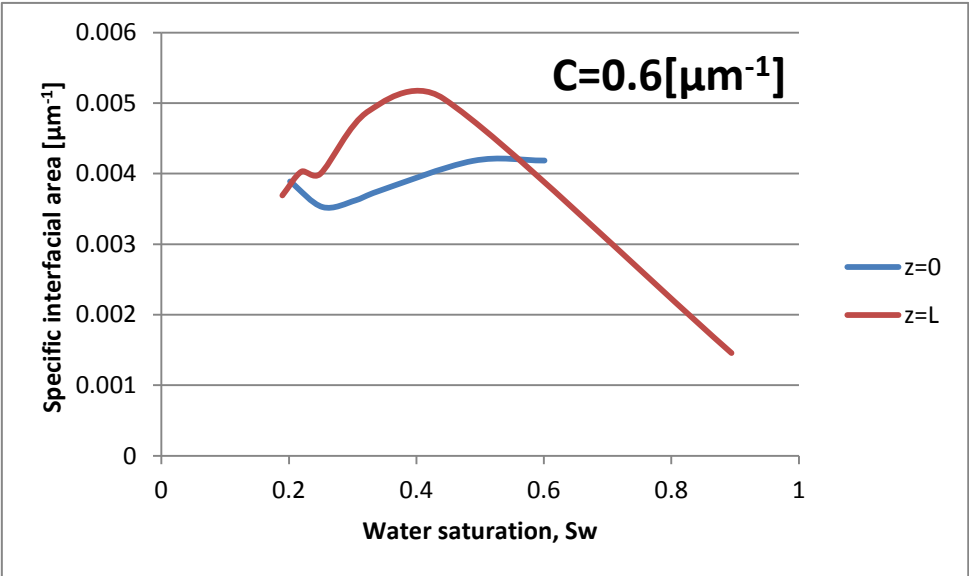***Figure 6.19:*** *The specific interfacial area between oil and water for invasion at z=L.*
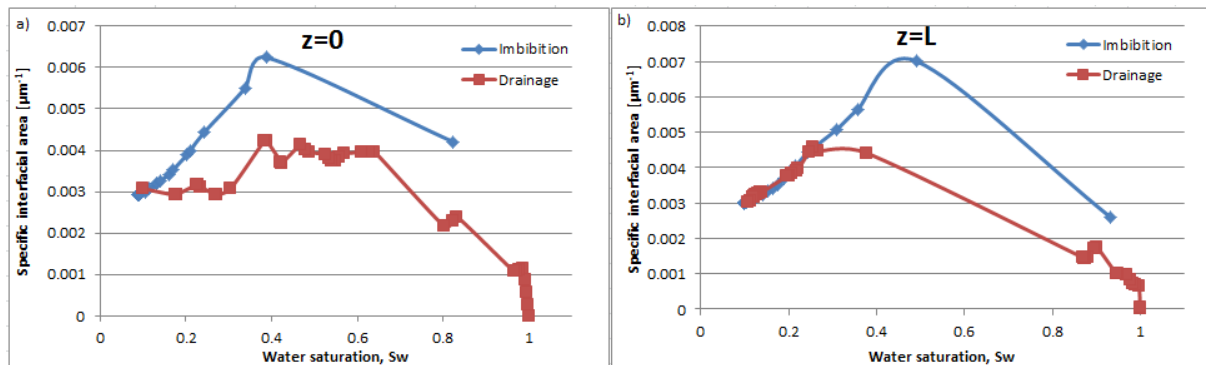


***Figure 6.20:*** *The specific interfacial area between oil and water for both drainage and imbibition at invasion a) z=0 and b )z=L.*

During imbibition it was mentioned that snap off and piston like invasion could occur. The piston like invasion will occur at the more favorable pressure, and also the interface is still present. Snap off will also undoubtedly give a higher interfacial area due to the splitting of the fluid phase. Furthermore as mentioned before Haines jump is an abrupt movement that occurs when the critical curvature has been exceeded. But because the Haines jump will result in a filling of the pore space, it will stop at a pore throat which was narrower then the previous one. This will intuitively give a smaller interfacial area then any of the other hysteresis events.

In the following three figures the water saturation and specific interfacial area for a constant curvature is plotted for invasion at z=0 and z=L. The curvature is chosen for C=0.5, C=0.6 and C=0.75, because these interface curvatures will give a value for all imbibition curves.



*Figure 6.21:* *The specific interfacial area between oil and water as a function of water saturation at constant interface curvature equal to $C=0.5[\mu m^{-1}]$*



*Figure 6.22:* *The specific interfacial area between oil and water as a function of water saturation at constant interface curvature equal to $C=0.6[\mu m^{-1}]$.*
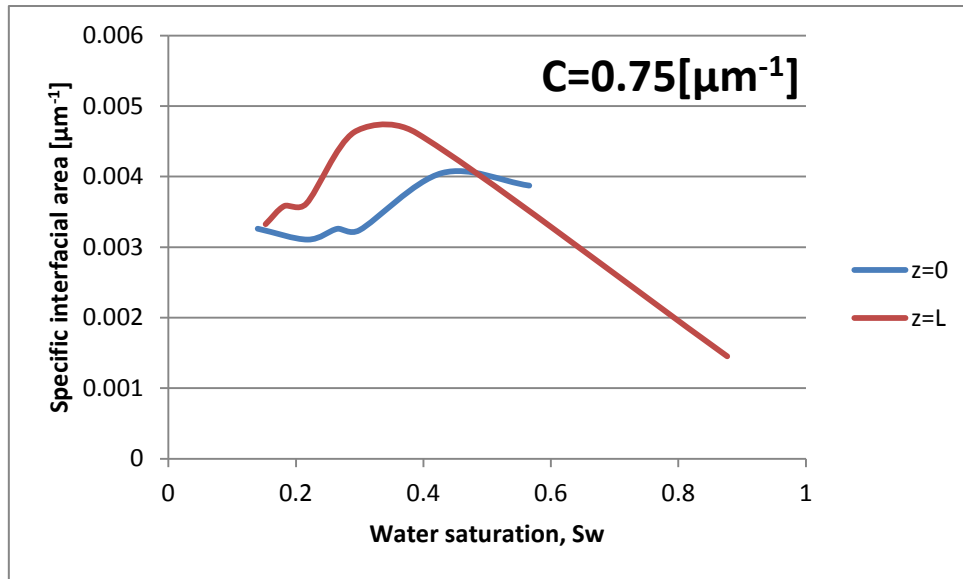
***Figure 6.23:*** *The specific interfacial area between oil and water as a function of water saturation at constant interface curvature equal to $C=0.75[\mu m^{-1}]$*

In all three figures of the constant interface curvature, the specific interfacial area for the invasion at z=0 and z=L do not coincide well. This is an indication that the difference between the capillary pressure curves for invasion at different sides cannot be eliminated by adding the specific interfacial area. Furthermore figure 6.24 show a three dimensional surface plot of the $P_c - S_w - a_{ow}$ relationship to compare with Porter et al. [2010]. Both surface plots in figure 6.24 have a slight convex shape. As shown in figure 5.3b) a slight bump in the surface plot can be an indication that there is hysteresis present. Both figure 6.24 and the previous three figures for constant interface curvature give result that including the interfacial area in the level set model does not eliminate hysteresis.
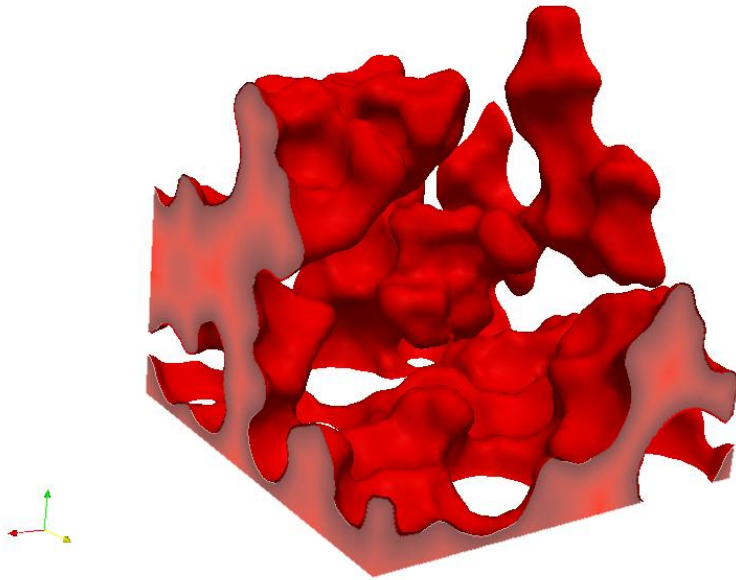
Figure 6.25 and 6.26 show a Paraview visualization of the oil displacement during drainage for z=0 and z=L, respectively. The details of the exact screenshot is shown in the upper left corner of the figure, and the interface curvature step is the same for the figures to be able to compare. Figure 6.25 shows a more stable displacement at this C step, compared to figure 6.26. Figure 6.25 shows what may seem as a small Haines jump in the upper left corner. Figure 6.26 has a much more drastic jump in the displacement and can be due to the pore connectivity the invasion of water at that direction encounters.
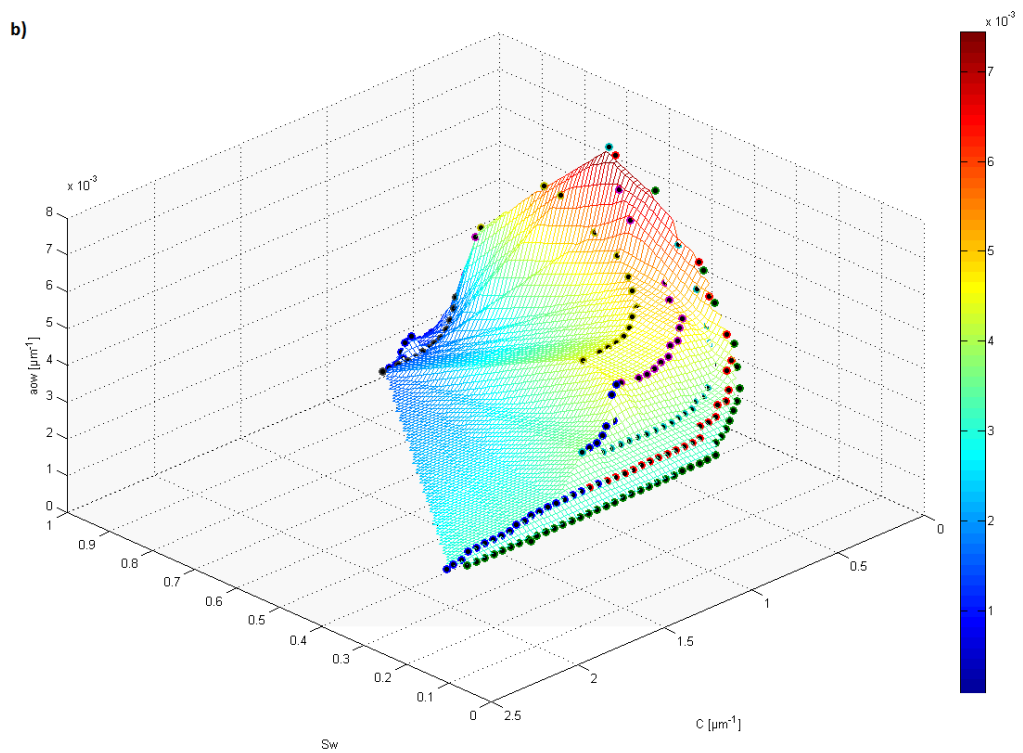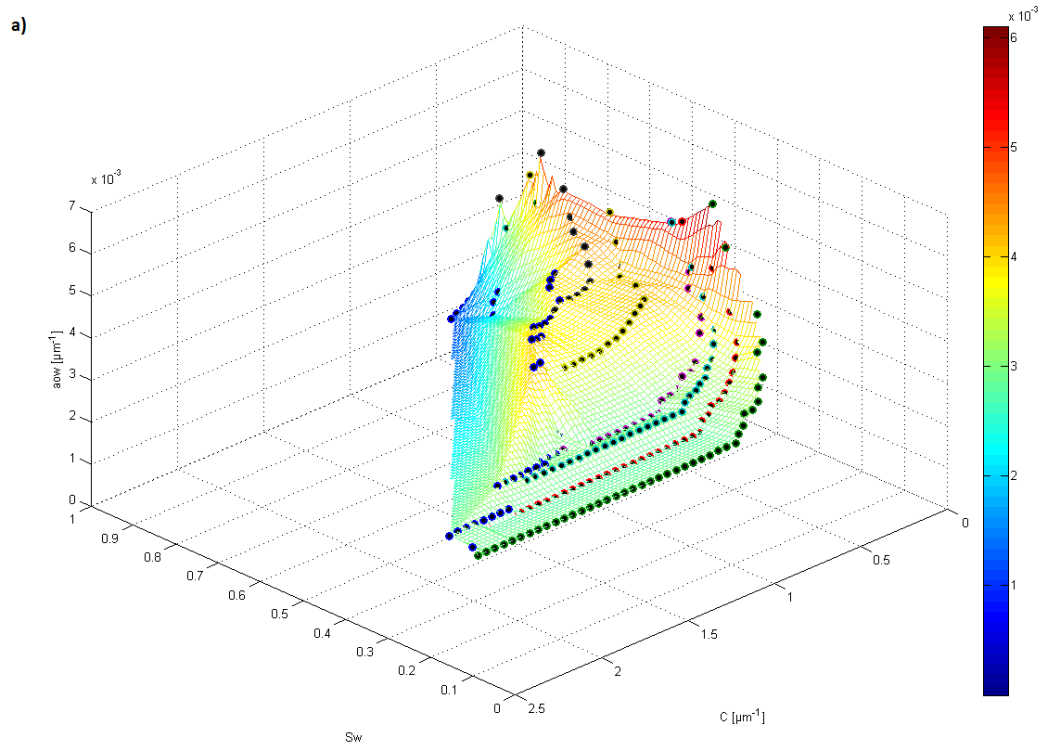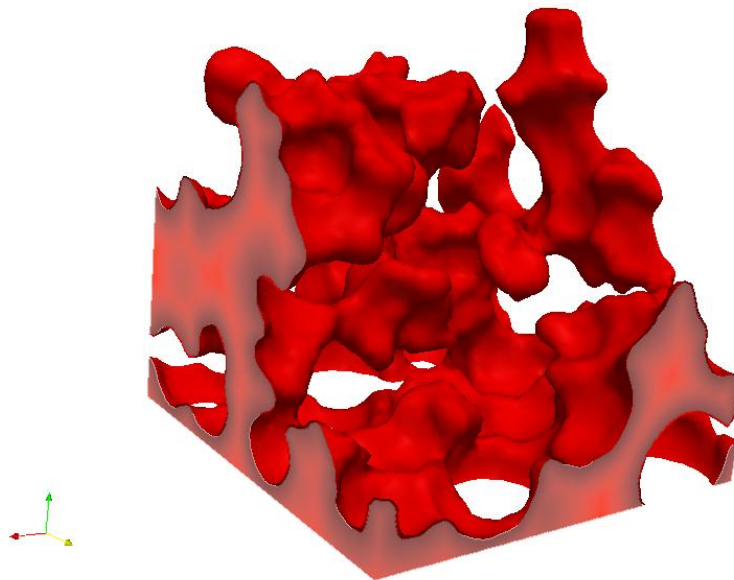
***Figure 6.24:*** *Surface plot of the relationship between the interface curvature, water saturation and interfacial area for a) z=0 and b) z=L.*
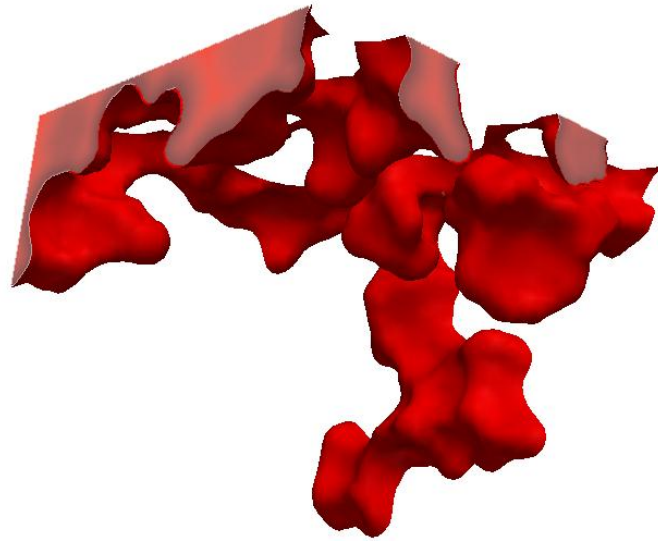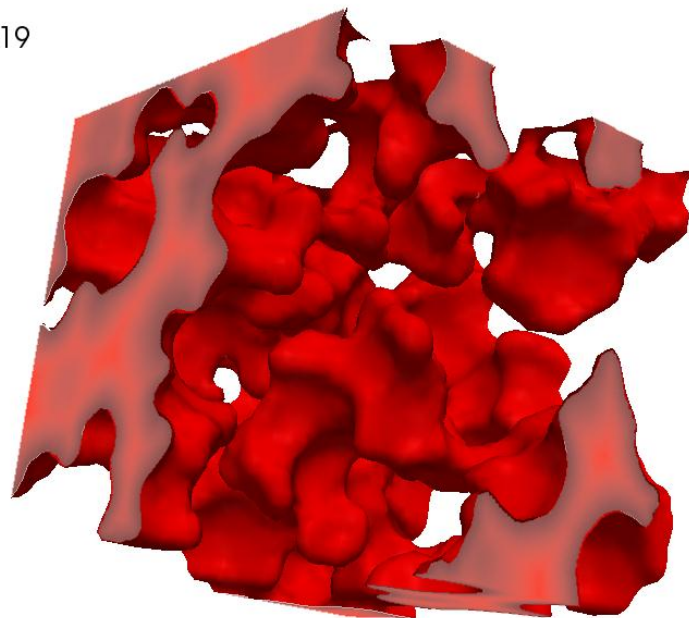
z=0
C=1
Sw=0.541



z=0
C=1.3
Sw=0.424



***Figure 6.25:*** *Oil displacement under drainage for a) C=1 b) C=1.3 for invasion at z=0.*

z=L
C=1
Sw=0.869

z=L
C=1.3
Sw=0.219

*Figure 6.26:* *Oil displacement under drainage for a) C=1 b) C=1.3 for invasion at z=L.*

Figure 6.27 till 6.30 show the Paraview visualization of the oil displacement during imbibition. The first two figures show the displacement for invasion at z=0, and the two subsequent figures for z=L. The visualizations for the figures are done for the interface curvature jump of only C=0.05 [$\mu m^{-1}$]. Figure 6.26 shows the imbibition curve starting at C=1.3, not a big change can be seen in the figure. However when comparing the two by quickly shifting them, a small jump in the interface can be observed. No snap off was observed in the figure for that curvature step, only piston like invasion occurred during the oil displacement. Same conclusion can be drawn for figure 6.28. Figure 6.29 does not show a snap off but at the bottom that where fluid is displaced there might have been a snap off. This could have been observed if a smaller curvature step was simulated. Figure 6.30 shows a clear occurrence of snap off, but again by quickly shifting the figures the piston like invasion is the one that occur the most in the figure. Actually it occur the most in all four figures. Additional figures of the drainage process for invasion at other sides are given in the Appendix. The most drastic jump in the saturation during drainage is for z=L, as can be seen from the drainage curves as well. The explanation can be that as oil is displaced in negative z-direction, at a certain point the critical curvature will get exceeded and also the gravity will yield to push the fluid through the porous media. All other invasions during drainage start on the horizontal plane.
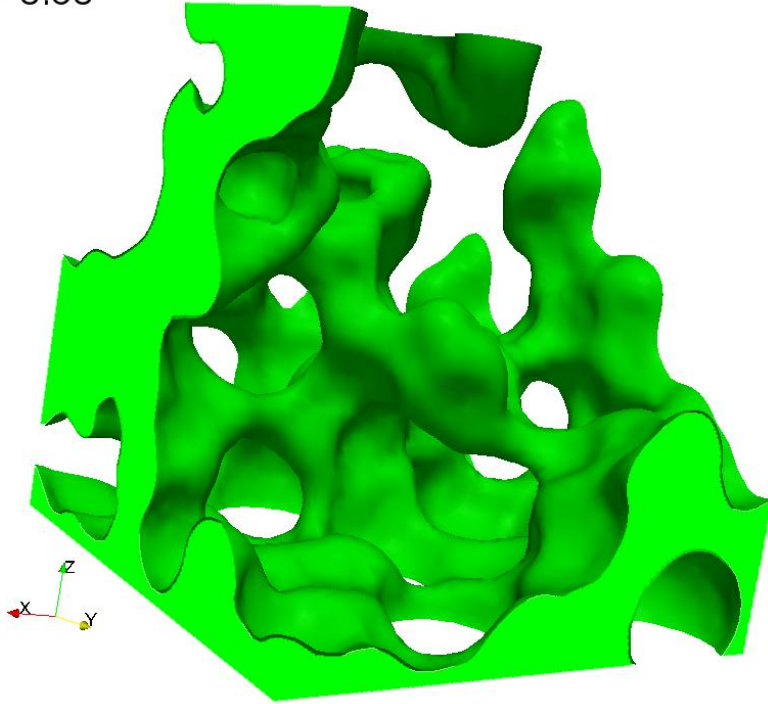
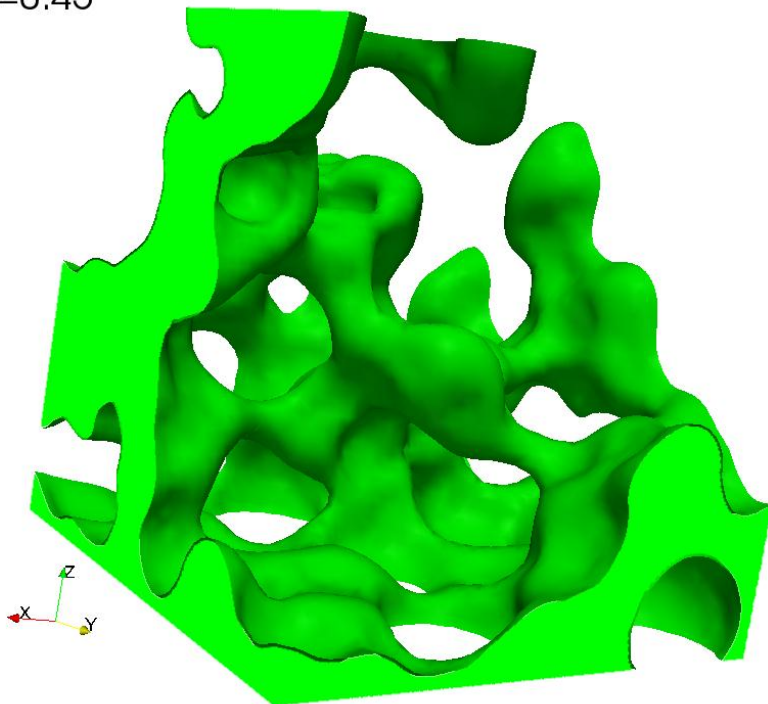Imbibition start at C=1.3
C=0.60
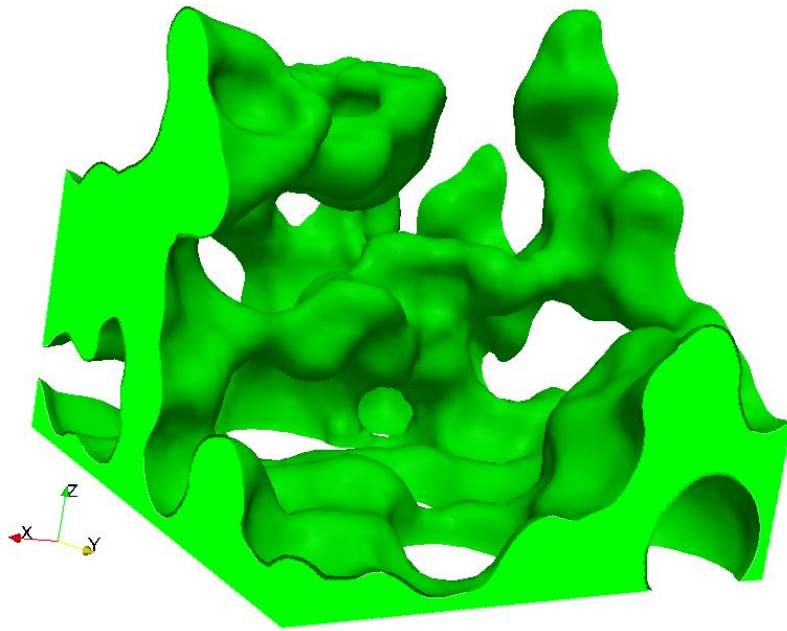


Imbibition start at C=1.3
C=0.55
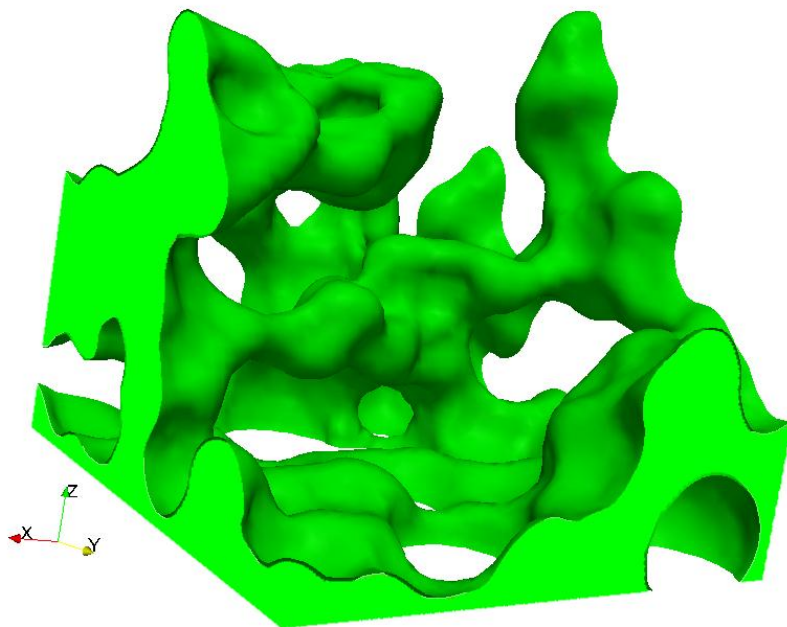


*Figure 6.27:* *Oil displacement under imbibition starting at C=1.3 for invasion at z=0*
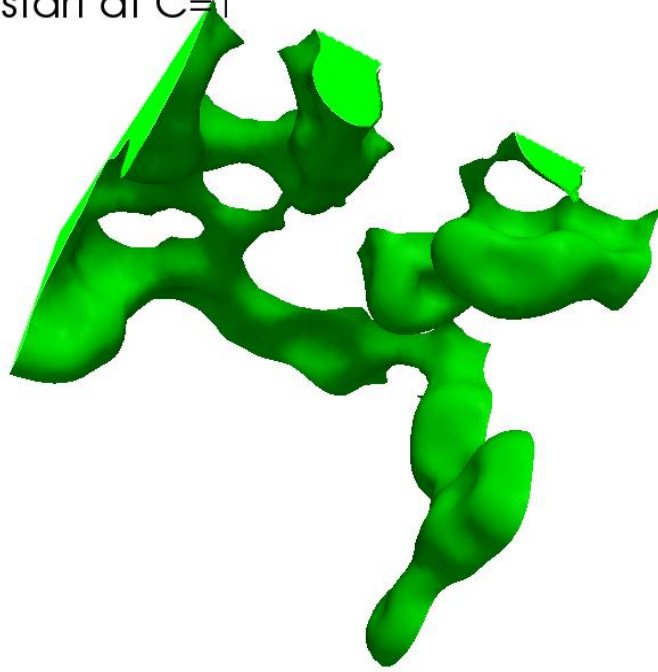
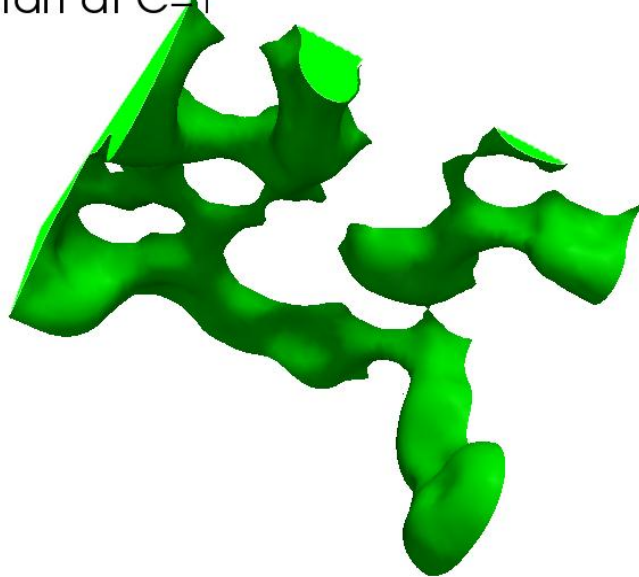Imbibition start at C=1.55
C=0.50



Imbibition start at C=1.55
C=0.45



*Figure 6.28:* *Oil displacement under imbibition starting at C=1.55 for invasion at z=0.*
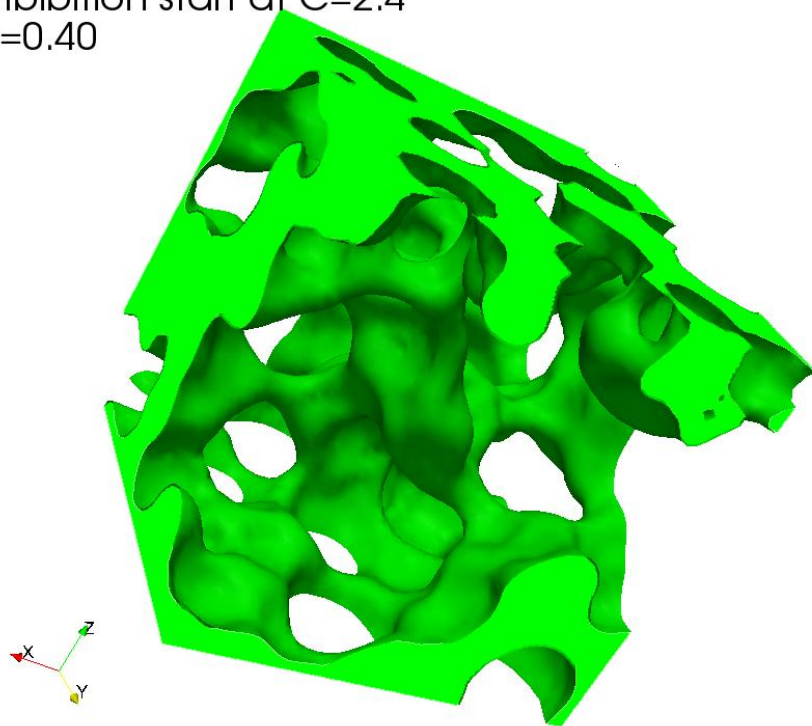
Imbibition start at C=1
C=0.45

Imbibition start at C=1
C=0.40
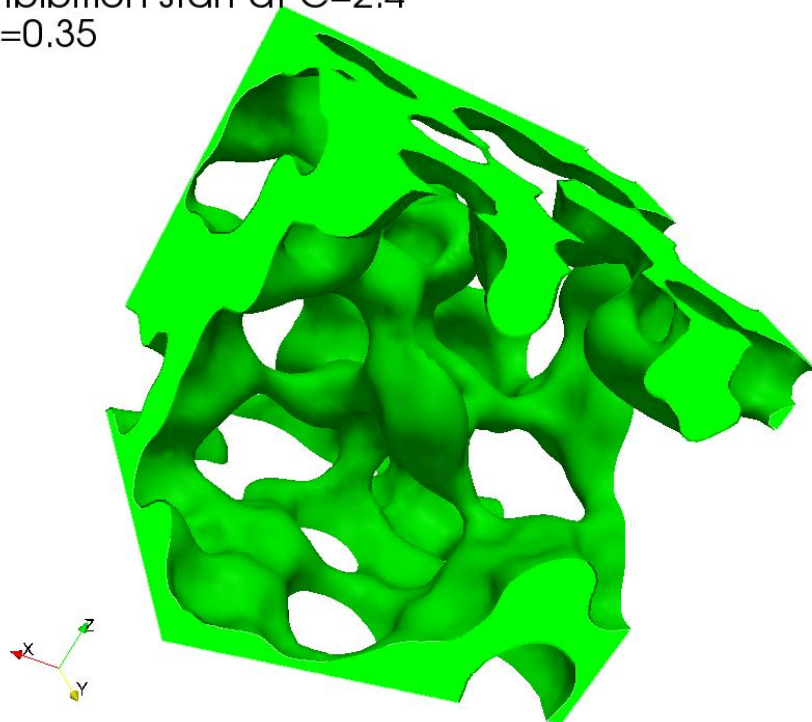
Figure 6.29: Oil displacement under imbibition starting at C=1 for invasion at z=L.

Imbibition start at C=2.4
C=0.40

Imbibition start at C=2.4
C=0.35

**Figure 6.30:** *Oil displacement under imbibition starting at C=2.4 for invasion at z=L.*

# CHAPTER 7

# CONCLUSION

The level set method is a great tool to examine the capillary-controlled displacement events in drainage and imbibition. The new method of using the Heaviside function to calculate the oil/water interfacial area is a powerful implementation to the level set model. We have shown that the level set model computation of the capillary pressure, water saturation and interfacial area between oil and water where in accordance with previous work done by Porter et al. [2010]. The model showed that the interfacial area between oil and water will be larger during imbibition than drainage. The model also showed that the capillary pressure curves for invasion at different sides of the sphere pack, will give different results during drainage. Furthermore the inclusion of the interfacial area between oil and water in the relationship between capillary pressure and water saturation did not eliminate these differences.

Additionally the Paraview visualization concluded that the most likely event to occur during imbibition was piston like invasion, which is in accordance with theory previously explained. Also the drastic jump in water saturation that was observed for z=L during drainage, was concluded to be due to the gravitational forces pulling the oil after critical curvature had been exceeded.

# RECOMMENDATIONS FOR FUTURE WORK

In this thesis great focus was set on determining whether the interfacial area between oil and water could eliminate hysteresis, by adding this parameter to the relationship between capillary pressure and water saturation. However the work has only looked at the result in vertical direction, hence the z-direction. Therefore our result is not completely conclusive and further simulation research for the horizontal directions should be addressed.

We also recommend further work with the level set model to verify if the inclusion of the interfacial area between any two immiscible fluids can aid to diminish or eliminate hysteresis. Also undergo simulations of drainage curves at different saturation points on the imbibition curves, and construct a surface plot of drainage and compare this result with the surface plot of imbibition constructed in our work. Also it is recommended to further work on examining the hysteresis events in Paraview by simulating with a smaller interface curvature step.

# APPENDIX

| $\varphi_{vs}$ | Interface = 0 | Solid = Positive | Void = Negative |
|---|---|---|---|
| $\varphi_{ow}$ | Interface = 0 | Oil = Negative | Water = Positive |

**Table A.1:** *Description of the signs the implicit functions calculates in the simulation for the different interfaces.*

**A.1** The three potential HJ ENO approximations to $\varphi_x^-$:

$$\varphi_x^1 = \frac{v_1}{3} - \frac{7v_2}{6} + \frac{11v_3}{6}$$

$$\varphi_x^2 = -\frac{v_2}{6} + \frac{5v_3}{6} + \frac{v_4}{3}$$

$$\varphi_x^3 = \frac{v_3}{3} + \frac{4}{6} - \frac{v_5}{6}$$

$v_1 = D^-\varphi_{i-2}$

$v_2 = D^-\varphi_{i-1}$

$v_3 = D^-\varphi_i$

$v_4 = D^-\varphi_{i+1}$

$v_5 = D^-\varphi_{i+2}$

**A.2** Central difference formulas used to discretize the spatial derivatives of $\phi$ in the curvature term:

**First order derivatives:**

$$(\phi_x)_{i,j,k} = \frac{\phi_{i+1,j,k} - \phi_{i-1,j,k}}{2\Delta x}$$

$$(\phi_y)_{i,j,k} = \frac{\phi_{i,j+1,k} - \phi_{i,j-1,k}}{2\Delta y}$$

$$(\phi_z)_{i,j,k} = \frac{\phi_{i,j,k+1} - \phi_{i,j,k-1}}{2\Delta z}$$

**Second order derivatives:**

$$(\phi_{xx})_{i,j,k} = \frac{\phi_{i+1,j,k} - 2\phi_{i,j,k} + \phi_{i-1,j,k}}{(\Delta x)^2}$$

$$(\phi_{yy})_{i,j,k} = \frac{\phi_{i,j+1,k} - 2\phi_{i,j,k} + \phi_{i,j-1,k}}{(\Delta y)^2}$$

$$(\phi_{zz})_{i,j,k} = \frac{\phi_{i,j,k+1} - 2\phi_{i,j,k} + \phi_{i,j,k-1}}{(\Delta z)^2}$$

**Second order mixed derivatives:**

$$(\phi_{xy})_{i,j,k} = \frac{\phi_{i+1,j+1,k} - \phi_{i-1,j+1,k} - \phi_{i+1,j-1,k} + \phi_{i-1,j-1,k}}{4\Delta x \Delta y}$$

$$(\phi_{xz})_{i,j,k} = \frac{\phi_{i+1,j,k+1} - \phi_{i-1,j,k+1} - \phi_{i+1,j,k-1} + \phi_{i-1,j,k-1}}{4\Delta x \Delta z}$$

$$(\phi_{yz})_{i,j,k} = \frac{\phi_{i,j+1,k+1} - \phi_{i,j-1,k+1} - \phi_{i,j+1,k-1} + \phi_{i,j-1,k-1}}{4\Delta y \Delta z}$$

In our case: $\Delta x = \Delta y = \Delta z$.

**A.3** Matlab code for the smeared Heaviside function:

Smeared Heaviside function:

```
b = 0;
eps = 1.5;
dx = 1;

i=0;
for phi_vs = -5:.05:5
    i=i+1;
    if phi_vs > (eps-b*dx)
    heavi_func(i) = 0;

    elseif phi_vs < (-eps-b*dx)
    heavi_func(i) = 1;

    else
    heavi_func(i) = 1/2 - phi_vs/(2*eps) - (b*dx)/(2*eps) +
(1/(2*pi)*sin(pi*(-phi_vs-b*dx)/eps));

    end

end

plot(-5:.05:5, heavi_func)
```
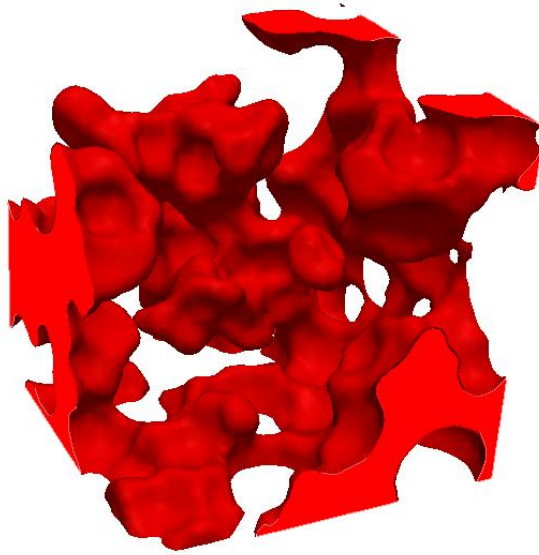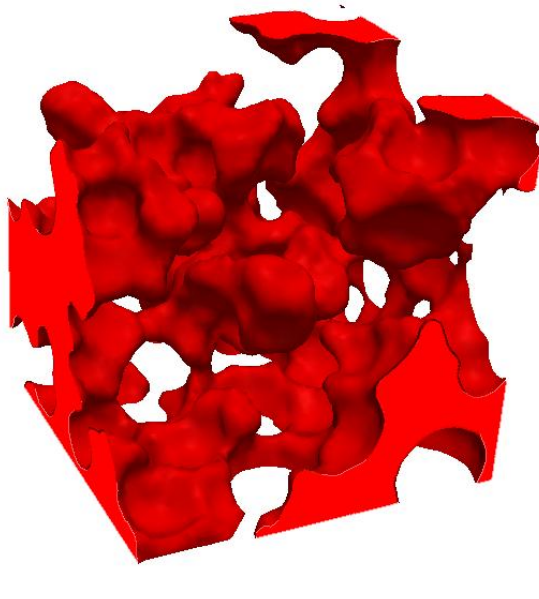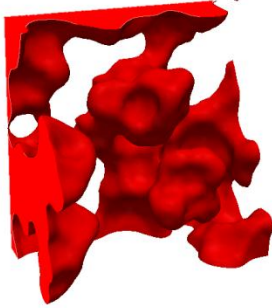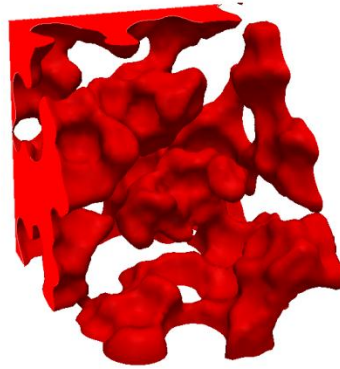
x=0
Sw=0.476065616
C=1



x=0
Sw=0.324192293
C=1.3



**Figure A.1:** *Oil displacement under drainage for a) C=1 b) C=1.3 for invasion at x=0.*
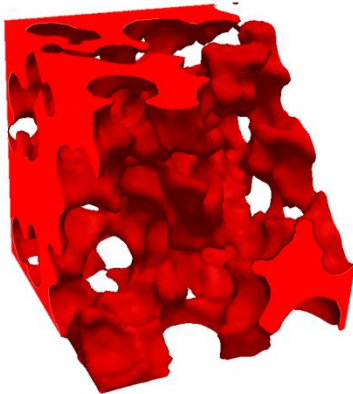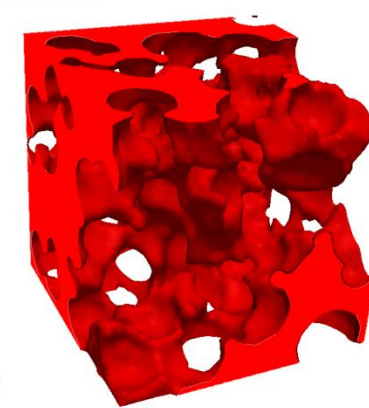
y=0
Sw=0.72582519
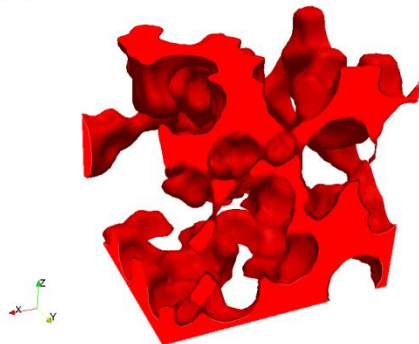C=0.7

y=0
Sw=0.509418206
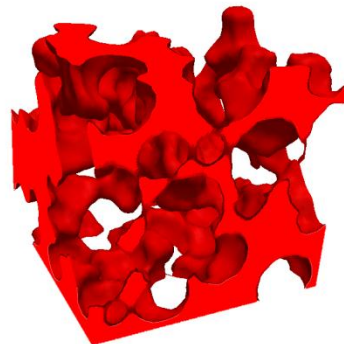C=1

y=0
Sw=0.17261898
C=2.2

y=0
Sw=0.087478627
C=2.5

***Figure A.2:*** *Oil displacement under drainage for four different C, at invasion y=0.*



y=L
Sw=0.528404
C=1

y=L
Sw=0.291470
C=1.3

***Figure A.3:*** *Oil displacement under drainage for a) C=1 b) C=1.3 for invasion at z=L.*

# REFRENCES

Ahmed, T.: *Working Guide to Reservoir Rock Properties and Fluid Flow* (2009) Gulf Professional Publishing: 49-50

Ahmed, T.: *Reservoir Engineering Handbook* (2010) Gulf Professional Publishing: 203-206

Asthana, R., Kumar, A., Dahotre, N.: M*aterials Processing and Manufacturing Science* (2006) Butterworth-Heinemann: 251-252

Barenblatt, G. I., V. M. Entov and V. M. Ryzhik: *Theory of Fluid Flows through Natural Rocks* (1990) Springer: 233-234

Barrera, A. E.: *History Matching by Simultaneous Calibration of Flow Functions* (2007) ProQuest: 91-92

Bear, J., Buchlin, J. M.: *Modeling and Applications of Transport Phenomena in Porous Media* (1991) Springer: 196-200

Bertotti, G. and I. Mayergoyz: *The Science of Hystersis: Mathematical modeling and applications, Volum 1* (2006) Academic Press: 735

Bhusan, B.: *Nanotribology and Nanomechanics II: Nanotribology, Biomimetics, and Industrial Applications* (2011) Springer: 556-557

Cerepi, A., L. Humbert and R. Burlot: *Pore-Scale Complexity of a Calcareous Material by Time-Controlled Mercury Porosimetry* (2000) Elsevier Science B.V.: 449-450

Culligan, K. A., D. Wildenschild, B. S. B. Christensen, W. G. Gray and M. L. Rivers: *Pore-scale characteristics of multiphase flow in porous media: A comparison of air-water and oil-water experiments* (2006) Advances in Water Resources 29: 227-238

Fanchi, J.: *Principles of Applied Reservoir Simulation* (2005) Gulf Professional: 29-31

Frette, O. I. and J. O. Helland: *A semi-analytical model for computation of capillary entry pressures and fluid configurations in uniformly-wet pore spaces from 2D rock images* (2010) Advances in Water Resources 33, 846-866

Held, R. J. and M. A. Celia: *Modeling support of functional relationships between capillary pressure, saturation, interfacial area and common lines* (2001) Water Resources 24: 325-343

Helland, J., and S. Skjaeveland: *Relationship between capillary pressure, saturation, and interfacial area from a model of mixed‐wet triangular tubes* (2007) Water Resour. Res., 43

Helland, J. O., Jettestuen, E., Hatzignatiou, D. G. and D. Silin: "*Three-dimensional level set modelling of capillary-controlled displacements in digital porous media*", abstract presented at 2011 AGU Fall Meeting in San Francisco, California, December 5-9, 2011.

Jerauld, G. R. and S. J. Salter: *The effect of Pore-Structure on Hysteresis in Relative Permeability and Capillary pressure: Pore-Level Modeling* (1990) Transport in Porous Media 5, 103-151

Joekar-Niasar, V., S.M. Hassanizadeh, L. J. Pyrak-Nolte and C. Berentsen  (2009*) Simulating drainage and imbibition experiments in a high-porosity micromodel using an unstructured pore network model*, Water Resour. Res., 45, W02430, doi:10.1029/2007WE006641

Joekar-Niasar, V., S.M. Hassanizadeh and A. Leijnse (2007*), Insights into the Relationship Among Capillary Pressure, Saturation, Interfacial Area and Relative Permeability Using Pore-Network Modeling*, Transp Porous Med., doi:10.1007/s11242-007-9191-7

Lenormand, R., C. Zarcone and A. Sarr: *Mechanisms of the displacement of one fluid by another in a network of capillary ducts* (1983) J.Fluid Mech., vol 135: 337-353

Lyons, W. and G. Plisga: *Standard handbook of Petroleum and Natural gas engineering* (2005) Gulf Professional Publishing: 38-40

Mohamad, A.: *Lattice Boltzmann Method: Fundamentals and Engineering Applications with Computer Codes* (2011) Springer: 2-3

Morrow, N. R.: *Physics and Thermodynamics of Capillary Action in Porous Media* (1970) Ind. Eng. Chem., 62 (6), pp 32-56

Muhammad, S.: *Flow and Transport in Porous Media and Fractured Rock: From Classical Methods to Modern Approaches* (2011) John Wiley & Sons : Chapter 10.1

Nosonovsky, M. and Bhushan, B.: Multiscale *Dissipative Mechanisms and Hierarchical Surfaces: Friction, Superhydrophobicity, and Biomimetics* (2008) Springer: 110-111

Osher, S. and R. Fedkiw: *Level Set Methods and Dynamic Implicit Surfaces* (2003) Springer-Verlag

Porter, M. L., D. Wildenschild, G. Grant, J. I. Gerhard (2010), *Measurment and prediction of the relationship between capillary pressure, saturation, and interfacial area in a NAPL-water-glass bead system*, Water Resour. Res., 46, W08512, doi:10.1029/2009WR007786

Porter, M. L., and D. Wildenschild: *Image analysis algorithms for estimating porous media multiphase flow variables from computed microtomography data: A validation study* (2010), Comput. Geosci., 14(1),15–30, doi:10.1007/s10596-009-9130-5

Porter, M. L., M. G. Schaap, and D. Wildenschild: *Lattice-Boltzmann simulations of the capillary pressure–saturation–interfacial area relationship in porous media* (2009) Adv. Water Resour., 32(11), 1632–1640, doi:10.1016/j.advwatres.2009.08.009.

Prodanovic, M. and S.L. Bryant: *Physics-driven interface modeling for drainange and imbibition in fractures* (2007) SPE 11044

Prodanovic, M. and S.L. Bryant: *Investigating pore scale configurations of two immiscible fluids via the level set method* (2006a) Computational Methods in Water Resources XVI.

Prodanovic, M. and S.L. Bryant: *A Level Set Method for Determining Critical Curvatures for Draiange and Imbibition* (2006b) J. Colloid Interface Sci. 304: 442-458

Rodriguez, E., M. Prodanovic and S. Bryant: *Contact line extraction and length measurements in model sediments and sedimentary rocks* (2012) J. Colloid Interface Sci. 368: 558-577

Schwartzstein R., Parker M.: *Respiratory Physiology: A Clinical Approach* (2005) Lippincott Williams & Wilkins: 51-52

Vafai, K.: *Handbook of Porous Media* (2009) CRC Press: 59-60

Vinci Technologies: *Determination of Capillary pressure & relative permeability curves with Refrigerated Centrifuge* page 2

Wendebourg, J. and J. W. Harbaugh: *Simulating oil entrapment in clastic sequences* (1997) Elsevier: 69-71

*The phenomenon of contact angle hysteresis*, Thermo Fisher Scientific: Process Instrument, Newington, USA. (www.**thermo**.com/e**Thermo**/CMA/PDFs/Various/File_9223.pdf).